PAUL SCHERRER INSTITUT

PSI

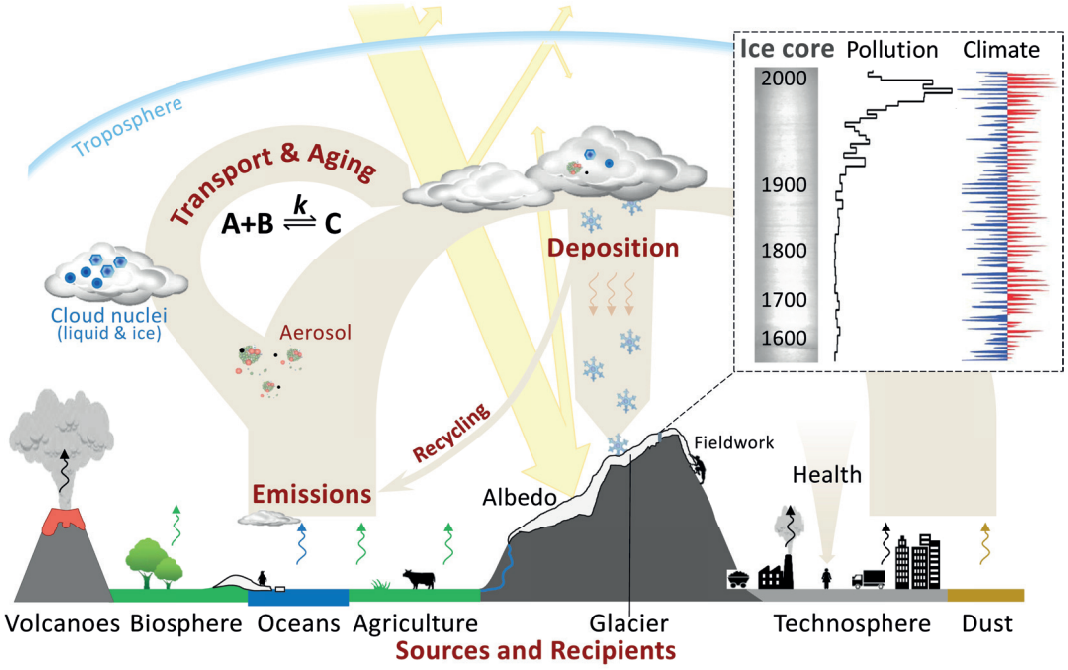

Annual Report 2016

Laboratory of Environmental Chemistry

Cover

In the troposphere, reactive gases and aerosol particles emitted by human activities such as energy production, mobility, agriculture, and by natural sources including volcanoes, the biosphere, oceans, and deserts. They undergo multi-phase chemical transitions, which are investigated under controlled laboratory conditions by the Surface Chemistry Group of the Laboratory of Environmental Chemistry (LUC). After transformation and transport in the atmosphere, aerosol particles and gases are eventually incorporated into snow and deposited on alpine glaciers. Ice cores from such glaciers are collected and analysed by the Analytical Chemistry Group of LUC to reconstruct air pollution levels, environmental conditions and climate variability in the past.

PAUL SCHERRER INSTITUT

Annual Report 2016

Laboratory of Environmental Chemistry

Editors
M. Schwikowski, M. Ammann

Paul Scherrer Institut
Laboratory of Environmental Chemistry
5232 Villigen PSI
Switzerland
Phone +41 56 310 25 05
www.psi.ch/luc
Reports are available: www.psi.ch/luc/annual-reports

TABLE OF CONTENTS

EDITORIAL

Last year the long tradition of publishing the Annual Report of the Laboratory of Radiochemistry and Environmental Chemistry (LCH) came to an end. This was the consequence of a decision of the PSI directorate to split the LCH into two: the Laboratory of Environmental Chemistry (LUC) and the Laboratory of Radiochemistry. To strengthen Environmental Research at PSI, LUC became part of the renamed Energy and Environment Research Division (ENE) and it was a great honour to me that I was appointed head of the laboratory as of 1 May 2016. LUC focuses on fundamental research and education for assessing the impact of human activities and natural processes on human health, environment and climate, and is organized in two groups. The **surface chemistry** research group headed by Markus Ammann investigates multi-phase chemical processes relevant for atmospheric chemistry and the **analytical chemistry** research group led by myself reconstructs environmental and climatic conditions from high-altitude glacier ice cores.

Encouraged by the positive feedback we have received over the years we decided to continue with publishing a compilation of our current work and I am proud to present here the first issue of the LUC Annual Report. We have streamlined the report by focusing on one-page abstracts about our work in progress, whereas additional news and information can be found on our webpage: https://www.psi.ch/luc/laboratory-of-environmental-chemistry-luc.

The year 2016 was characterized by the challenging disentangling of LCH infrastructure and personnel and by establishing LUC in the ENE research division. This transition was facilitated by already existing collaborations with the Laboratory of Atmospheric Chemistry (LAC) on atmospheric aerosol records in ice cores and with the Laboratory for Catalysis and Sustainable Chemistry (LSK) through joint operation of the Near-Ambient Pressure Photoemission endstation (NAPP) at the Swiss Light Source. To take full advantage of this facility, the surface chemistry group decided to give up the successful activities using the radiotracer ^{13}N for chemical kinetics and partitioning studies and focus more on molecular level studies of interface chemistry. At the same time the analytical chemistry group intensified the collaboration with LAC by developing a new approach for the chemical characterization of the organic fraction preserved in high alpine ice cores to reconstruct trends of atmospheric organic aerosols in Europe.

Already in the spring term we started with our LUC Friday-Seminars, which are organized by Theo Jenk. The first LUC excursion took us to the high-alpine research station Jungfraujoch, where we were competently guided through the facilities by Heinz Gäggeler and where we enjoyed the demonstration of ice core drilling given by Felix and Dieter Stampfli. In October we took advantage of the inspiring atmosphere at the seminar hotel Möschberg to grow together as LUC, enhance interaction between the groups, stimulate collaborations, and identify synergies during our first retreat. We concluded the year with a lot of fun at the Christmas party competition between the surface chemistry and the analytical chemistry group, organized with great enthusiasm by Peter Alpert and Pablo Corral Arroyo in the Waldhaus Brugg.

M. Schwikowski

Margit Schwikowski

SINGLE PARTICLE ANALYSIS OF URBAN AND MARINE AEROSOL

P. A. Alpert (PSI), P. Corral Arroyo (PSI & Univ. Bern), M. Ammann (PSI),
J. Dou, U. Krieger (ETHZ), B. Wang, S. Zhang (XMU)

Our aim is to quantify the mixing state of ambient aerosol particles impacted by urban outflow and marine emissions. Doing so will yield valuable insight into predicting aerosol composition, organic coating thickness, chemical and physical aging and light absorption properties.

Aerosol particles are solid or liquid matter suspended in our Earth's atmosphere. They are not a single compound, but rather a colloid with mixed multiple components of e.g. soot, organic and inorganic material [1]. Rarely is this mixing state quantified due to the fact that it requires observation of chemically distinct components within particles themselves. The technique, scanning transmission X-ray microscopy coupled with near-edge X-ray absorption fine structure spectroscopy (STXM/NEXAFS) is capable of chemically mapping single particles with sub-micrometer resolution [2]. Thus, their composition can be quantified by targeting only a few resonant peak absorption X-ray energies of soot (285.4 eV, carbon-carbon double bonding), organic matter (288.6 eV, carboxyl functional group) and non-carbonaceous (inorganic) matter which is determined from the absorption ratio at energies less than and greater than the ground state electron binding energy of the carbon atom (278 and 320 eV, respectively) [1, 3]. Statistical significance is obtained by investigating over 800 particles per samples assuring a precision greater than 5% at 99% confidence [3].

Aerosol particles were collected by the XMU group in the coastal South China Sea and analyzed with STXM/NEXAFS for mixing state. Two particle samples were selected which were collected about 200 km offshore of the Guangzhou-Hong Kong urban district in the South China Sea. The first termed "Continental-Marine" was taken from air originating from continential China which advected over an urban area and out to sea. The second sample termed "Offshore" was taken from air that remained offshore of China and did not travel over land. Particle samples were transported to the Paul Scherrer Institute (PSI) for STXM/NEXAFS investigation. The fraction of particles characterized by one or a mixture of components was derived from a publically available Matlab analysis package [1].

Fig. 1 shows that organic carbon (OC) and inorganic matter (In) is included in about 90% of all particles, which makes these components the most common. There were more particles with an elemental carbon (EC) component in the offshore sample than in the continental marine sample, which indicates a greater mixing time of marine air with urban outflow from coastal megacities. Fig. 1 also shows an example chemical map of the impacted particles which can give some insight into aerosol morphology [1, 3]. It is important to note that OC is frequently mapped on particle edges implying organic coatings. Inclusions of EC were identified in particle interiors and did not exhibit well-defined fractal geometry. Instead, they were collapsed and more spherical and always associated with other components, In and OC (Fig. 1). These results can be attributed to physical and chemical aging during their atmospheric lifetime.

Quantifying the presence and location of soot inclusions in particles is especially important for accurate representation of light absorption and scattering properties of ambient particles [1]. This preliminary mixing state dataset for urban-marine regions will be extended in future work and aid in radiative transfer calculations important for estimates of aerosol forcing. In addition it can constrain model estimates of aerosol flux, transport and chemical aging between these two environments.

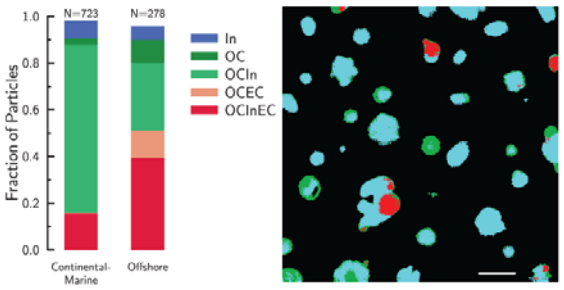

Fig. 1: Left - Fraction of particles identified as containing inorganic material (In), organic carbon (OC), elemental carbon (EC) and any mixtures of the three. The number of analyzed particles, N, is shown.
Right - An example chemical map of particles is indicating the mixing state of inorganic matter, organic matter and soot as cyan, green and red colors, respectively.

We acknowledge funding from the Swiss National Science Foundation (Grant 163074) and the Chinese Fundamental Research Funds for the Central Universities (Grant 2072160111). Sample collections were supported by NSFC Open Research Cruise (NORC 2015-05), funded by Shiptime Sharing Project of NSFC. This cruise was conducted onboard R/V "Dongfanghong II" by Ocean University of China.

[1] R. C. Moffet et al., Atmos. Chem. Phys., **16**, 14515-14525 (2016).
[2] J. Raabe et al., Rev. Sci. Instrum., **79**, 113704 (2008).
[3] Wang et al., J. Geophys. Res., **117**, D00V19, (2012).

OZONE PENETRATION IN VISCOUS MARINE ORGANIC AEROSOL

P. A. Alpert, P. Corral Arroyo, M. Ammann, B. Watts, J. Raabe (PSI), J. Dou, U. Krieger (ETHZ), S. Steimer (PSI & ETHZ), J.-D. Förster, F. Ditas, C. Pöhlker (MPIC), S. Rossignol, M. Passananti, S. Perrier, C. George (IRCELYON)

Ozone diffusion through viscous organic matter in aerosol particles – a proxy process representing aerosol aging - may be limited and thus, reactions will be substantially slower. In this study, ozone reactions were spatially mapped in submicrometer sized organic particles yielding quantitative measures of reacto-diffusive limitations.

Organic material derived from algal and bacterial exudates are aerosolized from the ocean along with sea salt [1]. The propensity of marine organic matter to be highly viscous at low relative humidity (RH) or cold conditions has not yet been investigated, although known to be important due to consequential limitations of gas diffusion and reaction through the organic matrix. Previous investigations related to the reaction of ozone with particle phase unsaturated compounds demonstrated that water vapor acts as a plasticizer to control viscosity, diffusivity and thus also reactivity [2]. Here, the reaction of ozone with Fe(II) in mixed submicron Xanthan gum and $FeCl_2$ particles was spatially mapped on a 35 nm scale using scanning transmission X-ray microscopy coupled with near edge X-ray absorption fine structure spectroscopy (STXM/NEXAFS) in a temperature and RH controlled environmental cell at the PolLux beamline of the Swiss Light Source (SLS). Xanthan gum was chosen as it is a surrogate for phytoplankton exudate material rich in polysaccharide. The $FeCl_2$ in particles reacts when exposed to ozone resulting in a transition from an Fe(II) to Fe(III) oxidation state. The STXM/NEXAFS technique is highly sensitive to the degree of iron oxidation at the Fe L-edge and the fraction of Fe(II), α, is able to be derived from absorption at selected X-ray energies of 707.8 and 709.5 eV indicating Fe(II) and Fe(III), respectively [3].

Fig. 1 shows radial profiles of α averaged over hundreds of particles in a humidified atmosphere where RH=40 and 80% during identical ozone exposure. Initial values were α=0.7 for both RH values. As ozone exposure continued over time, *t*, α was reduced more at particle perimeters than in particle interiors for both RH values. However, this gradient appears more exponential at RH=40% and more linear at RH=80%. When ignoring diffusion limitations of ozone and Fe, α should remain constant over the entire particle. However, this was not the case. The observed gradients imply a spatial scale characterizing iron and ozone molecular diffusion and reaction limitations (referred to as a reacto-diffusion length) which should be comparable to or less than the applied particle radius.

Depletion of Fe(II) due to ozone exposure occurs faster at 80% than for 40% RH. It was recently reported that Xanthan gum is hygroscopic and takes up water under these conditions [4]. Ozone is likely less soluble in water than in the organic matrix [2] and thus, greater water uptake at 80% RH would be expected to lead to lower reactivity. In turn, we suspect that water acts primarily as a plasticizing agent for the Xanthan gum polymers facilitating self-diffusion of both, Fe ionsand ozone. This should result in a greater reacto-diffusive length scale for RH=80% than at 40%. Our results demonstrate that humidity induced diffusivity changes can suppress reactions with condensed phase organic compounds, thus increasing their lifetime. Furthermore, spatial reaction gradients imply that bulk analysis of aerosol aging under the assumption of trace gas equilibrium with condensed phase organic aerosol may misrepresent aerosol aging reactions. This should also impact source apportionment and flux estimates using tracer compounds that may possibly react at higher humidities.

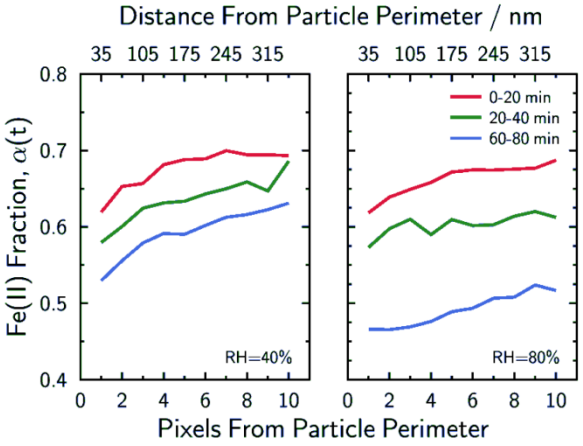

Fig. 1: Fraction of Fe(II) as a function of distance from particle perimeter, relative humidity (RH) and ozone exposure time.

We acknowledge funding from the Swiss National Science Foundation (Grant 163074).

[1] A. Laskin et al., J. Geophys. Res., **117**, D15302 (2012).
[2] S. S. Steimer et al., Atmos. Chem. Phys., **14**, 10761-10772 (2014).
[3] R. C. Moffet et al., J. Geophys. Res., **117**, D07204 (2012).
[4] K. W. Dawson et al., J. Geophys. Res., **121**, 11803-11818 (2016).

PHOTOCHEMISTRY OF IRON CITRATE IN ATMOSPHERIC AEROSOL PARTICLES

P. Corral Arroyo (PSI & Univ. Bern), J. Dou (ETHZ), P. A. Alpert, B. Watts, B. Sarafimov, J. Raabe (PSI), U. Krieger (ETHZ), M. Ammann (PSI)

Feedbacks between microphysics and photochemistry can be initiated by the absorption of UV-VIS light by iron citrate complexes in atmospheric aerosol particle proxies and are studied with a multidiagnostic approach. We elucidate photochemical reactions in single aerosol particles using scanning transmission X-ray microspectroscopy (STXM).

Iron complexes are important species in indirect photochemical oxidation of organic compounds in atmospheric particles. Fe(III) carboxylate complexes absorb light below about 500 nm, which is followed by ligand to metal charge transfer (LMCT). This results in the reduction of Fe(III) to Fe(II), oxidation of the carboxylate ligands and formation of H_2O_2. The latter reoxidizes Fe(II) to Fe(III) closing a catalytic cycle (Fig. 1). This process represents an important sink of organic acids in the troposphere [1, 2] and is potentially relevant as an aerosol aging process.

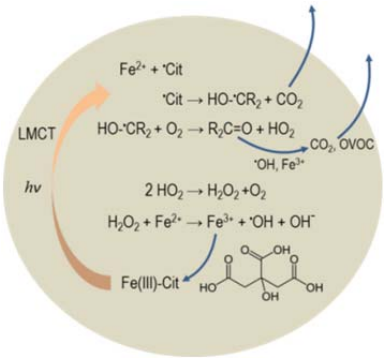

Fig. 1: Catalytic mechanism of iron citrate complexes initiated by UV-VIS light, followed by decarboxilation of the ligand and later by re-oxidation of Fe(II) to Fe(III) that closes the cycle.

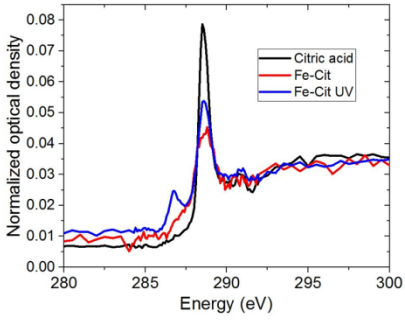

Fig. 2: Aerosol particle X-ray absorption spectra of citric acid and iron citrate (Fe-Cit). UV exposure to iron citrate (Fe-Cit UV) lasted 2 hours under nitrogen in dry conditions. These spectra are normalized to their area from 280-320 eV.

STXM enables quantification of carbon functional group composition [3] and iron oxidation state [4]. Fig. 2 demonstrates a new absorption peak at 286.3 eV characteristic of ketones after exposing citric acid particles containing iron citrate to UV light in dry N_2, where recycling of Fe(II) to Fe(III) does not occur. This is evidence in support of the decarboxylation reaction depicted in Fig. 1 to produce ketone containing products.

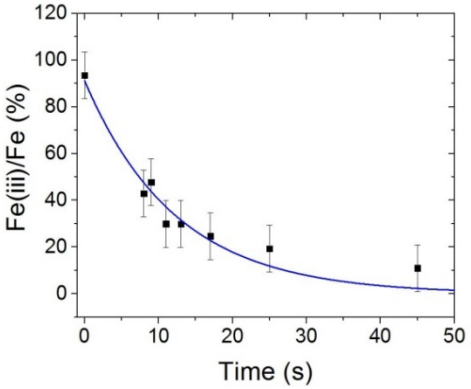

Fig. 3: Fe(III) fraction in citric acid particles containing iron citrate during UV irradiation under He and dry conditions. The line is an exponential fit to the data.

The oxidation state of iron was followed at the Fe L edge (spectra not shown) by employing the in situ environmental cell [3] and by using a procedure described by Moffet et al. [4] for analysis. The decay kinetics of Fe(III) under helium and UV light (375 nm, 350W/m^2) was 0.08 s^{-1} (Fig. 3) corresponding to a life time of 12 seconds. Similar decay kinetics was observed for the same system under oxygen and humidity, indicating that either the O_2 partial pressure was too low or the HO_2 or H_2O_2 escaped to the gas phase so that re-oxidation of Fe(II) to Fe(III) was not fast enough. This latter hypothesis is also supported by the fact that UV exposure beyond 1 minute did not result in additional degradation in presence of O_2. Further insight into this photochemistry will come from coated wall flow tube experiments and offline product analysis at PSI, as well as experiments in an electrodynamic balance at ETHZ.

We acknowledge funding from the Swiss National Science Foundation (Grant 163074).

[1] Weller, C. et al., Photochem. Photobiol. A, **268**, 24-36 (2013).
[2] George, C. et al., Top. Curr. Chem., **339,** 1-54 (2014).
[3] Steimer, S. S. et al., Atmos. Chem. Phys., **14**, 10761-10772 (2014).
[4] Moffet R.C. et al., J. Geophys. Res., **117**, D07204 (2012).

PHOTOCHEMISTRY OF IMIDAZOLES IN ATMOSPHERIC AEROSOL PARTICLES

P. Corral Arroyo (PSI & Univ. Bern), R. Aellig (ETHZ), S. Perrier, S. Dumas (IRCELYON), P. Rairoux (Univ. Lyon), C. George (IRCELYON), M. Ammann (PSI)

This work explores the photochemistry initiated by near UV light in the aerosol phase of imidazole-2-carboxaldehyde (IC) with different electron/H atom donors. By measuring HO_2 production we quantify radical production and obtain information related to the chemical mechanisms of these processes.

Photochemical processes may occur in the condensed phase of aerosols driven by light absorbing organic compounds (George et al., 2015). Photosensitizers are chromophores which produce triplet excited states that are reactive oxidants at wavelengths that would not allow direct photolysis. HO_2 radicals play an important role in the photochemistry of the atmosphere. This project studies the HO_2 radical production from the photochemistry of IC (Fig. 1) and citric acid (CA), shikimic acid, syringol, iodide and bromide as electron/H atom donors.

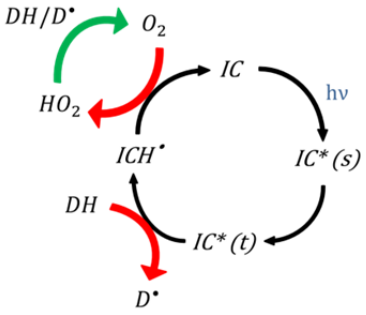

Fig. 1: Catalytic mechanism of IC with an H atom/electron donor, which goes through the triplet state and the ketyl radical, that involves the production and scavenging of HO_2 radicals.

Experiments were performed in a photochemical flow tube reactor at PSI, where IC/CA films were exposed to a stream of NO (up to 1 ppmv) in N_2/O_2 at atmospheric pressure and ratio. NO_2 production (resulting from the reaction of NO with HO_2 and thus our metric of HO_2 production) was observed under variable concentrations of the other four additional donors while keeping IC and the ratio between IC and the total amount of donors constant. The NO_2 and HONO produced was measured by the difference between NO signals of a chemiluminiscence detector (CLD), w/o a molybdenum converter (for conversion of NO_2 to NO) and w/o a HONO trap in line.

The results (Fig. 2 and 3) for the four donors added additionally to CA show a maximum in the HO_2 production at different concentrations for each of them. This behaviour could be explained by the fact that at some level of additional donor concentration, HO_2 production increases over that induced by CA alone (red arrow in Fig. 2 and 3) and that at higher donor concentration the donor or its oxidation product is acting as a sink for HO_2 (green arrow in Fig. 2 and 3). The position of the maximum is related to the rate coefficient of the reaction between the triplet state of IC and the donor (Tinel et al, 2014; and new measurements at IRCELYON (not shown)) and with the rate coefficients of the scavenging reactions of the triplet state and the ketyl radical.

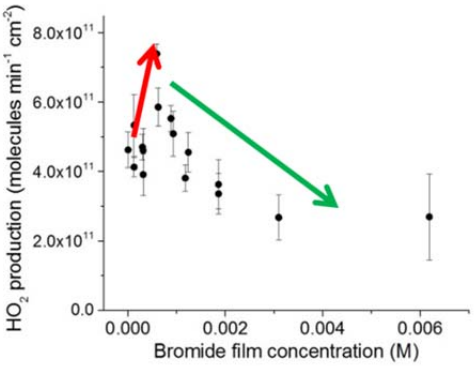

Fig. 2: HO_2 production for films with a constant amount of IC and CA and increasing concentrations of bromide.

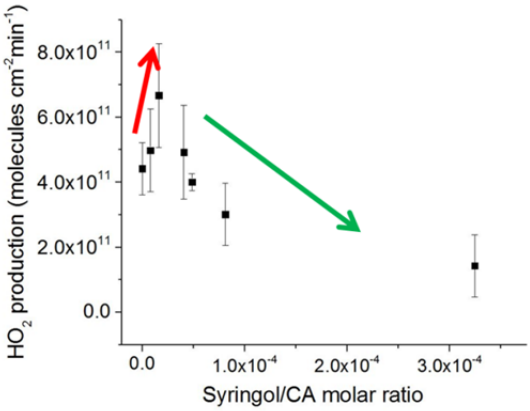

Fig. 3: HO_2 production for films with a constant amount of IC and CA and increasing concentrations of syringol.

Comparison of the behavior for the different donors allows to indirectly extract information about the elementary steps in the photocatalytic cycles and to upscale HO_2 production for atmospheric conditions.

We acknowledge funding from the Swiss National Science Foundation (Grant 163074).

[1] C. George et al., Chem. Rev. **115 (10)**, 4218-4258 (2015).
[2] L. Tinel et al., C. R. Chim. **17**, 801-807 (2014).

HOW DOES WATER PENETRATE THROUGH AN ORGANIC FILM?

X. Kong (PSI & Univ. Gothenburg), A. Habartova, E. Pluharova, M. Roeselova (Czech AS), C. Toubin (Univ. Lille 1), J. Pettersson (Univ. Gothenburg)

The adsorption and diffusion processes of water on an organic film are investigated by Molecular Dynamics (MD) simulations.

A large range of organic compounds can form films on airborne particular matter. Such films at the interface alter mass exchange between the gas and solid phases. Large organic molecules have been relatively well studied because of significant impacts of their films on gas uptake [1]. Short chain organics have less effect on uptake coefficients. This Molecular Dynamics (MD) study shows that even though the apparent uptake coefficient remains unchanged, the mass exchange between the gas phase and the condense phase is largely prohibited in presence of such films. Such new insights on water interactions with small organics is important for understanding atmospheric particles' behavior and for developing aerosol spray drugs because of large usage of short chain organics as solvents.

Fig. 1 (a) shows the system of interest, i.e. a snapshot of hexagonal crystalline ice coated by an *n*-butanol monolayer on two interfaces. Panel (b) shows the density profiles of water oxygen (in blue) and butanol atoms (oxygen in red, hydrogen in green and carbon in black) along the depth. According to the relative position, the carbon tails of butanol point away from the ice while the oxygen atoms of butanol are preferably in contact with the water layer, which indicates that the bonding between butanol and ice is thus occurring through the hydroxyl group. The formation of hydrogen bond is further confirmed after obtaining the binding energy and bond length distributions between butanol and water (not shown).

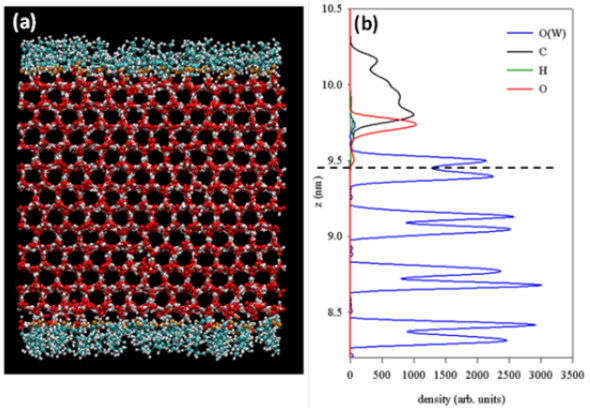

Fig. 1: (a) Prismatic side view of the hexagonal ice model with butanol coverage at 200 K; (b) water oxygen and butanol atoms density along the surface normal, z, sampled over a 100-ns simulation at 200 K. The bilayer-featured water oxygen peaks (blue) correspond to the hexagonal structure of ice. The dotted line marks the top layer (mid-plane).

Impinging water molecules were sent towards the interface to mimic molecular collisions. About 20% of incoming water molecules were scattered away directly in a few picoseconds after collisions, while the rest were trapped. Fig. 2 shows the diffusive movements of trapped H_2O as a series of density profiles in different simulation time. Right after collision, the trapped water molecules spread in a broad range in the z direction (4 ps). Already in the next snapshot at 8 ps the trapped water molecules start to accumulate towards the first ice layer, where a small peak is formed at the z position of about 9.7 Å. As time evolves, trapped water molecules continue to move towards to this region until the peak is stabilized from 32 ps. The peak at around 9.7 Å is at the same position as the oxygen atoms of butanol molecules, which is buried by the carbon tails. These water molecules are unlikely to desorb with less efforts compared to desorption from a neat ice surface.

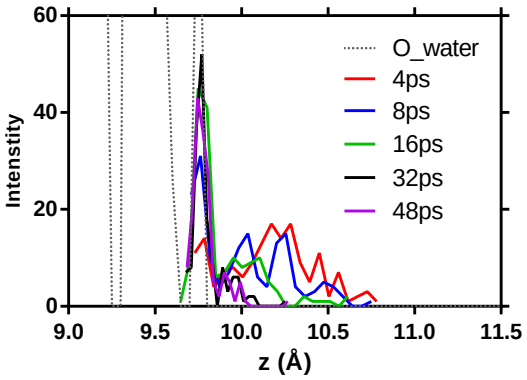

Fig. 2: Population distributions of trapped beam water in the z direction at different time.

The apparent trapping probability obtained in this simulation agrees nicely with previous molecular beam studies, but the close look into the process of diffusion in picosecond time scale indicates that the molecular exchange is actually prohibited that it cannot be seen macroscopically.

We acknowledge funding from the Swedish Research Council (Grant 2014-6924).

[1] J. F. Davies et al., PNAS, **110**, 8807-8812 (2013).
[2] X. R. Kong et al., J. Phys. Chem. B, **118,** 13378-13386 (2014).

NITRATE PHOTOCHEMISTRY ON TiO_2 PROBED BY AMBIENT PRESSURE XPS

F. Orlando (PSI), A. Waldner (PSI & ETHZ), X. Kong (PSI & Univ. Gothenburg), L. Artiglia, T. Bartels-Rausch, M. Ammann (PSI)

Photocatalytic degradation on the surface of mineral dust is thought to affect the concentration of nitrogen oxides (NOx) in the atmosphere. In this study, we provide direct spectroscopic evidence of the fates of nitrate and reduced nitrogen species at the surface via in situ near ambient pressure X-ray Photoelectron Spectroscopy (XPS) using TiO_2 as a mineral dust proxy.

The uptake and photo-transformation of NO_x on TiO_2 is suggested to play a crucial role in atmospheric chemistry, being a potential source of radicals and radical precursors. Photocatalytic degradation of NO_x on TiO_2 under UV irradiation yields HNO_3 as a final product, with a conversion rate depending on the detailed conditions of relative humidity and light intensity [1]. The uptake of nitric acid on dust particles is considered as a sink for atmospheric NO_x, but its photolysis as a potential renoxification process has been debated in the last years [2]. Also, TiO_2 photocatalysis of NO_2 has been identified as a potential source of HONO [3], which is not only a harmful species but also a precursor of reactive OH radicals, which participate in ozone and secondary organic pollutants production. On the other hand, the identification of adsorbed nitrogen oxides species and their role in mediating the photo-assisted degradation of organic compounds on TiO_2 is still lacking sufficient information. We present here the first results of a study of the surface chemical evolution of nitrogenated species on TiO_2 using near ambient pressure XPS.

A TiO_2 nanopowder sample (Degussa P25) was pretreated with HNO_3 and drop-casted on the sample holder. The approach adopted in the present experiment allowed probing the process of nitrate photolysis in absence of gas phase NO_x. Fig. 1 shows the N 1s core level spectrum of the as-prepared sample treated with HNO_3 (red spectrum). The most abundant surface species is NO_3^-, as expected, but other components appear in the spectrum, which are attributed to NO_2^- and other reduced nitrogenated species. A UV laser was used to irradiate the sample while monitoring the surface species. The nitrate degradation previously reported in at least two independent investigations was not observed (purple spectrum). The NO_3^- photoemission intensity remained unchanged after one hour of irradiation: we hypothesize that nitrate reduction does not occur due to the presence of O_2, in the gas phase, which is an electron scavenger. A background pressure of O_2 was indeed used to prevent carbon accumulation on the measured sample spot. On the other hand, we suspect that previously reported nitrate degradation was mediated by organic contaminations and/or related to gas phase photochemistry.

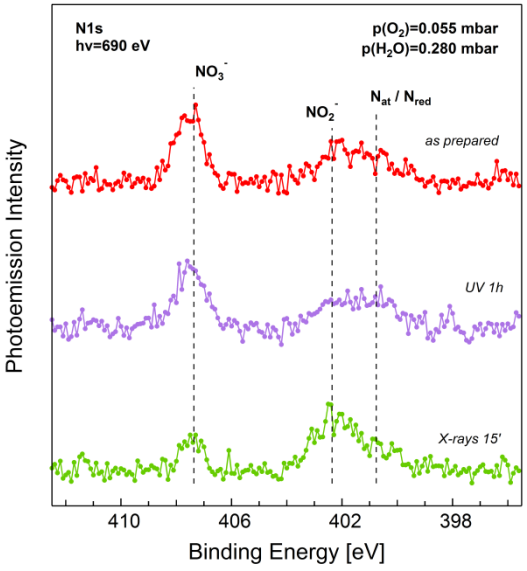

Fig. 1: N 1s core level photoemission spectra of TiO_2 powder sample pretreated with a 0.1 M solution of HNO_3.

Further investigations in this sense will be performed by adding a photosensitizer allowing for electron transfer mechanism to the conduction band of TiO_2. Fig. 1 also shows the strong beam-induced effect (green spectrum). Exposure of the sample to X-rays leads to substantial reduction of the nitrate peak and to a buildup of intensity in the region attributed to reduced nitrogenated species. The pronounced X-ray induced reaction represents an additional complication when characterizing NO_x photochemistry with XPS. We are also performing offline photolysis experiments of nitrate on TiO_2 to confirm the higher than expected stability against indirect photolysis. The results will deepen our understanding on the mechanism for the formation of surface-adsorbed species and its atmospheric implications.

We acknowledge funding from the Swiss National Science Foundation (SNF grant No. 149492).

[1] J. S. Dalton et al., Environ. Pollut. **120**, 415-420 (2002).

[2] M. Ndour et al., Geophys. Res. Lett. **36**, L05816 (2009).

[3] J. M Langridge et al., Atmos. Environ. **43**, 5128-5131 (2009).

THE FATE OF HYDROGEN CHLORIDE ON ICE

X. Kong (PSI & Univ. Gothenburg), A. Waldner (PSI & ETHZ), F. Orlando, L. Artiglia, M. Birrer, M. Ammann, T. Bartels-Rausch (PSI)

Adsorption, dissociation and diffusion of HCl at the ice surface and beyond: The decade-long puzzle of the fate of HCl on ice is largely solved in this core-level photoelectron spectroscopic study.

The interaction of HCl with ice got intensive attention since the discovery of the ozone hole three decades ago. Several key processes are still open to debate, such as acid dissociation and diffusion on and in ice. The current picture becomes even more blurred at temperatures approaching the melting point of ice because the formation of the Quasi Liquid Layer (QLL) and its influence on dissociation and diffusion remain poorly understood.

In the Near Ambient Pressure Photoemission (NAPP) end station, single crystal ice was grown at -20°C. Molecular HCl and dissociated Cl^- were distinguished by the different chemical shifts of Cl 1s and Cl 2p photoelectron peaks. This work provides the first ever observation of undissociated HCl on ice at such high temperatures. Depth profiles of molecules, ions and the ratio of them were obtained by varying the kinetic energy (KE) of photoelectrons by varying the incident photon energy, which result in different inelastic photoelectron mean free path (IMFP), and thus probe depth. The depth profiles are plotted in Figure 1, with fits by a three-layer model.

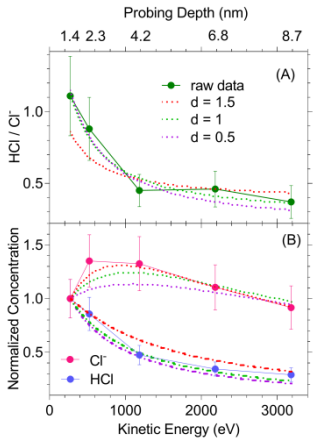

Fig. 1: Depth profiles of (A) HCl/Cl^- ratio and (B) normalized HCl and Cl^- concentrations. Dashed and dotted lines the fitting results.

Molecular (HCl) and ionic (Cl^-) chloride show a different vertical distribution. Undissociated molecules were exclusively detected in the topmost layers. This is in agreement with the instantaneously occurring dissociation of HCl once the molecule finds 2 dangling hydrogen atoms [1]. In contrast, ionic Cl^- shows an ascending trend in the upper surface layers up to about 2.3 nm probing depth, which suggests that Cl^- accumulates in the sub-surface region. This observation agrees with previous flow tube experiments that have shown continuous uptake of HCl by ice under comparable conditions [2, 3], which was proposed as a process accompanied by dissociation. The three-layer model is described in detail in the upcoming publication.

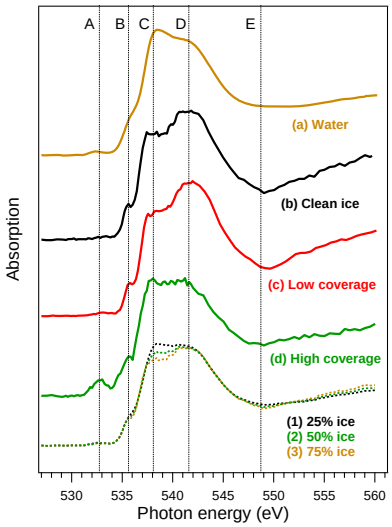

Fig. 2: Oxygen K-edge NEXAFS spectra.

The HCl induced surface disorder of the hydrogen bonding network is also directly probed. Figure 2 shows the oxygen K-edge near edge X-ray fine structure (NEXAFS) spectra of (a) liquid water, (b) neat ice, ice with (c) low and (d) high HCl pressure, and a series of linear combinations of ice and water. Liquid water and solid ice can be discriminated by the ratio of the main- (C) and the post-edge peak (D). Low HCl coverage ($< 5 \cdot 10^{-6}$ mbar) seems not to disorder the ice surface. At high coverage (d) ($7.5 \cdot 10^{-5}$ mbar, same as the depth profile experiments, near phase transition from solid HCl doped ice to liquid HCl solution), the NEXAFS line partially transits from the solid ice feature to the liquid water feature. A series of linear combinations of liquid water (A) and clean ice (B) with various fractions are shown, where the 25% ice + 75% water combination captured the best similarity to the HCl induced disordered ice surface.

We acknowledge funding from the Swiss National Science Foundation (Grant 149629) and the Swedish Research Council (Grant 2014-6924).

[1] J. P. Devlin et al., Nature, 417, 269-271 (2002).
[2] McNeill, V. F., et al., PNAS, 103, 9422-9427 (2006).
[3] Huthwelker, T., et al., J. Phys. Chem. A, 108, 6302-6318 (2004).

LABORATORY BASED APXPS ICE MEASUREMENTS @ LBL

A. Waldner (PSI & ETHZ), T. Bartels-Rausch, M. Ammann (PSI), H. Bluhm (LBL)

A laboratory based ambient pressure X-ray photoelectron spectroscopy (APXPS) set-up was further developed enabling measurements of trace gas uptake to ice.

Uptake of trace gases on ice can modify the composition of the atmosphere [1, 2]. Previous studies demonstrate that the uptake of some trace gases on ice can be quantified using Langmuir-type adsorption isotherms [3], while others show a different uptake behavior [1]. Processes leading to the observed differences in uptake are not well understood. A better knowledge of the uptake process is necessary to improve the interpretation of concentration profiles in ice cores and atmosphere/climate models. APXPS enables us to directly observe the interaction of a trace gas on ice and to quantify the uptake.

The objective of this project is to adapt a laboratory based (in contrast to synchrotron based) APXPS setup at Lawrence Berkeley National Laboratory (LBL) for experiments, which can be used to examine the adsorption of trace gases on ice at a molecular level. The advantage of a lab based APXPS system is the lower photon flux, which minimizes beam damage, and also the ease of access in contrast to synchrotron based XPS. The disadvantage is the lack of tunability of the photon energy and longer acquisition times for spectra.

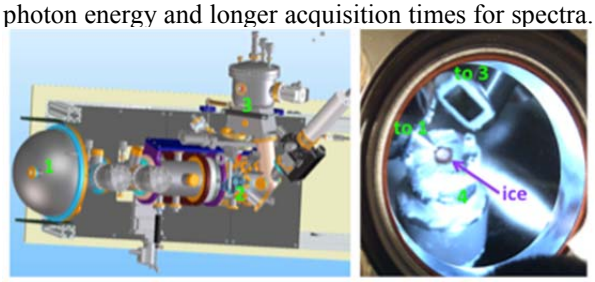

Fig. 1: Sketch and picture of APXPS lab set-up.

Fig. 1 shows the newly adapted setup, consisting of a SPECS APXPS detector (1), experimental cell (2), X-ray source (3) (hv: ~1476 eV) and the sample holder (4) for growing ice samples attached from below. The sample holder consists of several parts, including a temperature controlled (Peltier) copper substrate. The ice samples are grown in-situ by condensing water vapor from the gas phase onto the cooled substrate. Typically, a ~2 mm thick ice film is formed after ~1 hour of growth. By increasing the temperature of the substrate the ice sample is equilibrated. The stable ice is characterized prior to exposure to the respective trace gases (in this case propionaldehyde).

Fig. 2 shows a typical C1s spectrum of propionaldehyde on ice. It shows 4 distinct features, which can be assigned to gas phase and adsorbed propionaldehyde. The ratios of the respective peak areas (2:1) show that there is no beam damage of the propionaldehyde and that it adsorbs intact on the ice.

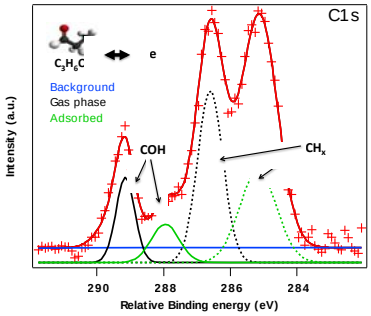

Fig. 2: Exemplary C1s spectrum of the interaction between propionaldehyde (C_3H_6O) and ice.

The left side of Fig. 3 shows isotherms of propionaldehyde on ice. The lines represent fits following Langmuir-type adsorption. Based on the measured values of the Langmuir constant of isotherms at different temperatures, we can determine the adsorption enthalpy (slope of fit in graph of right side of Fig. 3) to be ~ -25 kJ/mol (-6.25 kcal-mol).

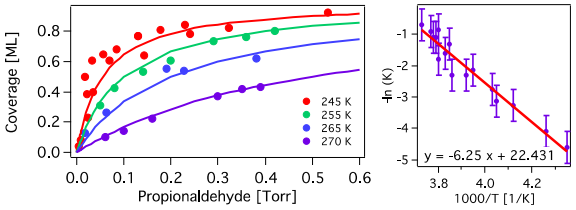

Fig. 3: Left: Isotherms of propionaldehyde adsorbed on ice. Right: Using Langmuir constants from Isotherms measured at different ice temperatures the adsorption enthalpy can be derived.

We acknowledge funding from the Swiss National Science Foundation (Grant # 149629). This work was supported by the Director, Office of Science, Office of Basic Energy Sciences, and by the Division of Chemical Sciences, Geosciences and Biosciences of the U.S. Department of Energy at LBNL under Contract No. DE-AC02-05CH11231.

[1] T. Huthwelker et al., Chem. Rev., **106**, 1375-1444 (2006).
[2] F. Dominé et al., Science, **297**, 1506-1510 (2002).
[3] M. Ullerstam et al., Farad. Discuss., **130**, 211-226 (2005).

AFFINITY OF PROPIONIC ACID FOR THE AQUEOUS SOLUTION - AIR INTERFACE

S. Chen (PSI & ETHZ), F. Orlando, L. Artiglia (PSI), P. Corral Arroyo (PSI & Univ. Bern), M. Ammann (PSI)

Organic acids are wide-spread on aqueous environmental interfaces. Their properties at the interface may play a crucial role in cycling of reactive atmospheric trace constituents [1, 2]. Here, we obtained surface sensitive spectroscopic insight for aqueous propionic acid and sodium propionate solutions.

We investigated aqueous solutions using liquid jet X-ray photoelectron spectroscopy (LJXPS) coupled with near edge X-ray absorption fine structure spectroscopy (NEXAFS) at the NAPP end-station at the SIM beamline at the SLS [3] to further understand surface chemical composition, molecular environment and orientation of propionic acid and the conjugate base propionate ions.

Fig. 1 (right axis) shows the measured functional group C 1s photoemission (PE) signal intensity for aqueous solutions of propionic acid and sodium propionate against their bulk mole fraction. The experiments indicate that the neutral carboxylic acids are much more enriched at the surface as compared to the corresponding carboxylate ions of the sodium salt solution.

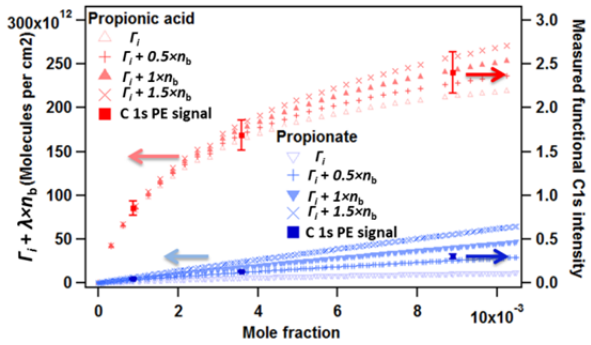

Fig. 1: Measured (right y-axis) and simulated (left y-axis, eq. (1)) functional group C 1s PE signal for photon energy $h\nu$ = 450 eV for propionic acid and propionate against their bulk mole fraction (error bar: *10%*).

The measured photoemission intensity (I) is sensitive to both, the number density of molecules at the surface itself, Γ_i, and bulk molecules with a concentration n_b residing within the probe depth, characterised by the inelastic mean free path of the photoelectrons. Γ_i, also referred to as the surface excess, can be obtained from surface tension data via the Gibbs equation [4]. Therefore, the PE intensity can be approximated by [5, 6, 7]:

$$I = A\,(\Gamma_i + \lambda \times n_b) \qquad (1)$$

where A denotes a constant related to the overall measurement efficiency. Equation (1) was used to simulate the data in Fig. 1 with Γ_i derived from literature surface tension data. Since λ is not well established for liquids [8], we test the sensitivity with *λ=0.5nm, λ=1nm, and λ=1.5nm*. The results show that with *λ=1nm*, the value expected for inelastic scattering of electrons in a solid with similar density, the measured data are reproduced fairly well. Thus, these experiments confirm the linear relationship of the C 1s PE intensity with surface excess [7].

C K-edge NEXAFS spectra of propionic acid solutions recorded at 0.2, 0.5, 1.0 M, are shown in Fig. 2. The sharp resonance at 289.1 eV is due to the C 1s-to-π* transition of the carboxyl carbon. The broader spectral feature in the region between 292 and 304 eV is assigned to the 1s-to-σ* transition. The π* intensity slightly increases with concentration. Whether this is related to recently discovered photochemistry involving a triplet excited state [8] or to increasingly upward orientation [7] requires further analysis.

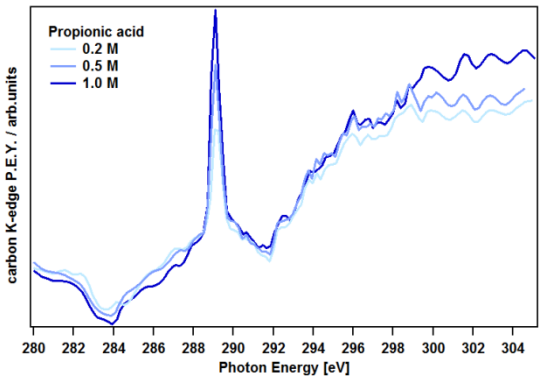

Fig. 2: Partial electron yield NEXAFS spectrum of propionic acid solutions at 0.2, 0.5, 1.0 M aqueous solution.

We acknowledge funding from the Swiss National Science Foundation (Grant 149492).

[1] S. Rossignol, et al., Science, **353**, 699-702 (2016).
[2] K. Stemmler, et al., Atmos. Chem. Phys., **8**, 5127-5141 (2008).
[3] M. A. Brown, et al., Surf. Sci., 610, 1-6 (2013).
[4] Adamson, et al., Physical chemistry of surfaces, 6th edition, Wiley: New York (1997).
[5] J. G. Pruyne, et al., J. Phys. Chem. C, **118**, 29350-29360 (2014).
[6] M.-T. Lee, et al., J Phys. Chem. A, **119**, 4600-4608 (2015).
[7] M.-T. Lee, et al., J. Phys. Chem. A, **120**, 9749-9758 (2016).
[8] N. Ottosson, et al., J. El. Spectr. Rel. Phen., **177**, 60-70 (2010).

FENTON'S CHEMISTRY AT THE LIQUID/GAS INTERFACE

L. Artiglia, F. Orlando (PSI), S. Chen (PSI & ETHZ), P. Corral Arroyo (PSI & Univ. Bern), M. Ammann (PSI)

The reaction between Fe^{2+} solutions and hydrogen peroxide (H_2O_2), commonly known as Fenton's reaction, produces either highly-valent Fe species (ferryls, FeO^{2+}) or Fe(III) and OH radicals as reaction intermediates [1, 2], which may be preferentially formed at the interface [3]. We exploited the surface sensitivity of x-ray photoelectron spectroscopy (XPS) to try to identify chemical species at the liquid/gas interface.

Fenton's chemistry is of wide interest, due to the presence of Fe(II) and peroxides both in vivo [4] and in the environment (atmosphere, water, and soils) [5], but remains poorly understood in terms of the details. The preferential formation of either ferryls or Fe(III) and OH radicals influences the course of oxidative chemistry [6]. Recently, it was demonstrated that microdroplets of a Fe(II) solution react promptly with H_2O_2 from the gas phase to form mono- and poly-iron high valent species [3]. The reaction at the interface was 10^3-10^4 times faster than the same reported in bulk aqueous media, maybe due to the incomplete hydration shell of Fe(II). By means of liquid jet XPS and x-ray absorption spectroscopy (XAS), performed at the near ambient pressure photoemission (NAPP) endstation, we measured in-situ the reaction of Fe(II) aqueous solutions with gas phase H_2O_2.

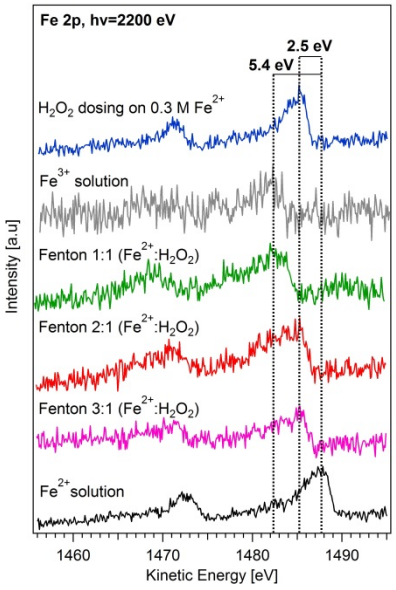

Fig. 1: XPS of the Fe 2p core-level.

Moreover, we analyzed aqueous solutions of Fe(II) and Fe(III), to be used as references, and mixtures of Fe(II) and H_2O_2, prepared ex-situ and injected into the experimental chamber. The goal was to compare the XPS of the references to those of Fenton's reagents having different [Fe(II)]/[H_2O_2] ratios. By dosing H_2O_2 from the gas phase, we aimed at investigating the reaction at the liquid/gas interface, i.e. where the formation of FeO^{2+} should be maximized [6]. Fig. 1 shows a collection of preliminary XPS of the Fe 2p core-level acquired at the Phoenix beamline using tender x-rays (2200 eV excitation energy). The concentration of the Fe(II) and Fe(III) solutions were 0.3 M. A clear change is observed when H_2O_2 reacts ex-situ with Fe(II), because the peaks shift negatively, i.e from the kinetic energy corresponding to Fe(II) to that of Fe(III). Furthermore, the peaks broaden, in agreement with the formation of other reaction products, e.g. iron hydroxyls [7]. When H_2O_2 is dosed from the gas phase in situ, the XPS evolves differently: it shifts by ca. 2.5 eV from the Fe(II) reference, and the spin orbit splitting decreases by 2.0 eV, becoming comparable to that of Fe(III). The Fe L_3 XAS preliminary results are also showing a modification of the lineshape, suggesting that new species are formed. Further experiments are needed to reproduce the data acquired so far, and associate the spectral features to a reaction intermediate.

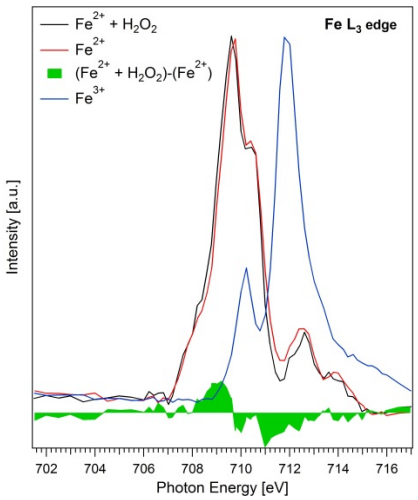

Fig. 2: Spectrum of the Fe L_3 absorption threshold.

[1] H. J. H. Fenton, J. Chem. Soc. Trans., **65**, 899-910 (1894).

[2] T. Logager, et al., Inorg. Chem., **31**, 3523-3529 (1992).

[3] S. Enami, et al., Proc. Natl. Acad. Sci. USA, **111**, 623-628 (2014).

[4] T. A. Rouault, Science, **325**, 676-677 (2009).

[5] E. Harris, et al., Science, **340**, 727-730 (2013).

[6] M. T. Green, et al., Science, **304**, 1653-1656 (2004).

[7] A. D. Bokare, et al., J. Hazard. Mater. **275**, 121, (2014).

SURFACE INTERMEDIATE IN THE OXIDATION OF BROMIDE BY OZONE

S. Chen (PSI & ETHZ), L. Artiglia, F. Orlando (PSI), P. Corral Arroyo (PSI & Univ. Bern), M. Ammann (PSI)

The heterogeneous reaction of ozone with bromide ions in ocean water or sea-spray aerosol occurs through an acid catalyzed mechanism involving a $BrOOO^-$ complex as an intermediate [1]. Here, we provide direct evidence for the formation and stabilization of $BrOOO^-$ at the surface by LJXPS.

The oxidation of bromide by ozone is one of the important reactions initiating the emission of halogen compounds from aqueous solution that later drives O_3 depleting chemistry in the troposphere [2]. We investigated the reaction of gas phase ozone (O_3) with aqueous NaBr solutions in-situ by means of liquid jet x-ray photoelectron spectroscopy (LJXPS) performed at the near ambient pressure photoemission (NAPP) endstation at the SIM beamline at SLS. Fig. 1a shows the liquid-microjet (inner quartz nozzle) with the gas dosing system (outer metal nozzle). The Br 3d core level (doublet with a spin-orbit splitting of ca. 1.0 eV) collected from a NaBr solution before and during dosing the gas, is shown in Fig. 1b and 1c. When dosing O_2, no changes are observed, whereas while dosing a mixture of O_2 and O_3, the peaks broaden in the high binding energy (BE) region of both the $3d_{5/2}$ and $3d_{3/2}$. The new species (marked in pink) is shifted positively by 0.7 eV as compared with the BE of Br^-. The spectra of other conceivable stable oxidation products of Br^- (not shown) demonstrate that the new peak can be associated neither to BrO^- nor to BrO_3^- [2].

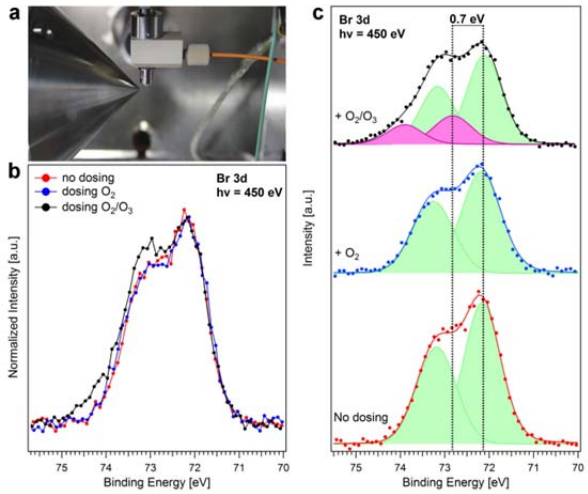

Fig. 1: (a) Photograph of the liquid-microjet in action; (b) Br 3d spectra of 0.125 M NaBr at hv = 450 eV; (c) Deconvolution of the Br 3d spectra of 0.125 M NaBr solution in vacuum (bottom), in O_2 (middle), and in O_3/O_2 (top).

The spectrum of a 0.08 M solution of BrO^- shifts positively by 2.1 eV and that of a 0.125 M solution of BrO_3^- shifts positively by 7.0 eV as compared with the BE of Br^-. Therefore, the new component in the Br 3d region can be related to the $BrOOO^-$ complex.

Br 3d were also probed at different excitation energies (hv): 350 eV, 450 eV and 650 eV (Fig. 2a). Because higher excitation energy corresponds to a higher kinetic energy of the emitted photoelectrons, this experiment allows probing increasing information depths. The deconvolution of the core-level peaks allows us to calculate the area of the component associated to the $BrOOO^-$ complex at the three selected energies. The areas are then normalized to the area of condensed phase of O 1s, which is used as an internal reference. The Br 3d/O 1s intensity ratio is shown in Fig. 2b. Its value does not change significantly passing from 276 to 376 eV photoelectron kinetic energy, whereas it drops by a factor of about 2 when the kinetic energy is increased further by 200 eV. This means that the $BrOOO^-$ species stays preferentlially at the liquid-vapor interface.

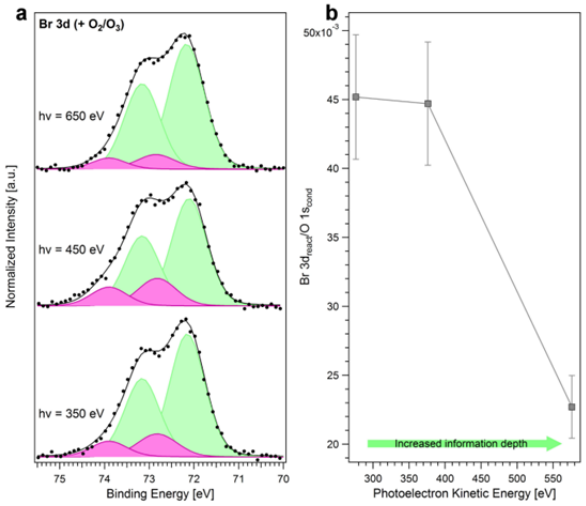

Fig. 2: (a) Br 3d spectra of 0.125 M NaBr solution dosing O_2/O_3 at different hv depth; (b) Br 3d PE signal intensity normalized by the area of condensed phase O 1s PE signal as a function of the hv.

We acknowledge funding from the Swiss National Science Foundation (Grant 149492).

[1] Q. Liu, et al., Inorg. Chem., **40**, 4436-4442 (2001).
[2] S. Wang, et al., Proc. Natl. Acad. Sci., **112**, 9281-9286 (2015).
[3] I. Gladich, et al., J. Phys. Chem. A, **119**, 4482-4488 (2015).
[4] T. Sasaki, et al., J. Chem. Phys., **71**, 4601-4610 (1979).

COMPARING OZONE UPTAKE IN SALT SOLUTIONS

J. Edebeli (PSI & ETHZ), M. Ammann (PSI), A. Gilgen (ETHZ), S. Chen (PSI & ETHZ), T. Bartels-Rausch (PSI)

In this study, we investigated the multiphase reaction of ozone with bromide in aqueous solution at 0°C. The aim is to observe and parameterize the uptake of ozone while accounting for the effects of the solutes in the solution. This is a study of the proxy reaction for a larger project on the reactivity of contaminants in snow and ice.

Halogen activation via ozone (O_3) uptake is an important process in the lower atmosphere in both warm and cold climates [1, 2], where concentrated brine solutions can be found in aerosols, salt flats or brine pockets on land and on sea ice [3 – 5]. The activated halogens trigger a variety of reactions, which alter the oxidative capacity of the atmosphere, which in turn affects the lifetime of atmospheric pollutants. In this report, we present a summary of a study comparing the uptake of O_3 over sodium bromide (NaBr) solution and a solution containing NaBr and sodium chloride (NaCl) in a rectangular trough flow reactor at 0°C described before [6]. Chloride is the most abundant halide in sea salt deposits and aerosols, but its reactivity with O_3 is much lower than that of bromide and iodide. The study focuses on bromide reactivity and shows lower ozone uptake in the NaBr/NaCl mixture than in the pure NaBr solution. This difference can be explained by reduction in ozone solubility (salting out) in the mixture.

Both solutions contained 0.125 M NaBr, and the mixture contained additional 0.55 M NaCl. 10 ml solution was used for each experiment. The pH of pure NaBr solution was 5.6 ± 0.1 and the mixture was 5.8 ± 0.1. The gas flow was cooled and humidified before delivery to the trough. The flow rate through the trough was 400 ml/min with a makeup flow for the ozone analyser of 600 ml/min, N_2, added after the trough. The O_3 concentration was monitored using a Teledyne API 400 analyzer.

The O_3 concentration ($[O_3]$) from the bypass is the maximum $[O_3]$ sent to the reactor. The $[O_3]$ from the trough corresponds to the concentration left after uptake of O_3. The conversion from O_3 loss to uptake (γ_{obs}) has been described in previous studies (see [6] and references there in).

The γ_{obs} was compared with a model that accounts for the effect of the salts on the solubility and diffusivity of O_3, the bulk reactive rate coefficient, and a parameterization of the reactive surface uptake of O_3. The model was fit in parallel to data from this study and another data set at 1°C (not shown), by using the Langmuir constant, K_{Lang}, and surface reaction rate coefficient, k_s^I, as free variables. The model is of the resistance model format [7, 8].

Fig. 1 shows the measured ozone uptake over NaBr solution and NaBr/NaCl mixture at 0 °C as a function of $[O_3]$ (dots) and model predictions (lines). The saturation behaviour at high $[O_3]$ indicates the presence of surface driven uptake especially at low atmospherically relevant $[O_3]$. The ozone uptake in the mixture, though with a higher concentration of halide ions, has a lower ozone uptake compared to the pure NaBr solution. This difference can be explained by the reduced solubility of ozone [9], and increased viscosity of the solution with the added NaCl [10]. The uptake predicted by the model for NaCl/NaBr solution is lower than the measured results because the model only considers the contribution of Br^- to the reactive uptake in addition to uncertainties in the parameters. The measured γ_{obs} are consistent with Oldridge and Abbatt's study with a NaBr/NaCl mixture, but lower Br^- concentration at pH 1.95 [11].

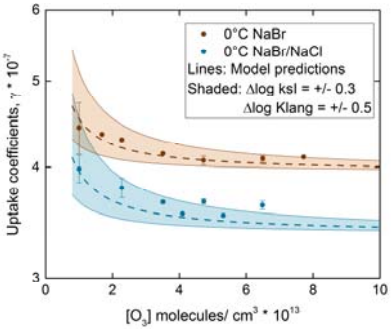

Fig. 1: γ_{obs} (dots) and model predictions (lines) as a function of ozone concentration. The shaded area has an applied Δlog of k_s^I of ±0.3 and Δlog of K_{Lang} of ±0.5 [8]. Each experiment was conducted independently at least twice.

We acknowledge funding from the Swiss National Science Foundation (Grant 155999).

[1] L. A. Barrie, et al., Nature, **334,** 138-141 (1988).
[2] K. Hebestreit, et al., Science, **283**, 55-57 (1999).
[3] W. R. Simpson, et al., Chem. Rev, **115**, 4035-4062 (2015).
[4] W. R. Simpson, et al., Atmos. Chem. Phys, **7**, 4375-4418 (2007).
[5] Abbatt, J. P. D., et al., Atmos. Chem. Phys, **12**, 6237-6271 (2012).
[6] M. T. Lee, et al., J. Phys. Chem. A, **119,** 4600-4608 (2015).
[7] B. J. Finlayson-Pitts, et. al, Chemistry of the upper and lower atmosphere, Academic Press, 156-167 (2000).
[8] M. Ammann, et al., Atmos. Chem. Phys, **13,** 8045-8228 **(**2013).
[9] S. Weisenberger, et al., AIChE Journal, **42**, 298-300 (1996).
[10] H. Ozbek, et al., ACS 29th SE Regional meeting, (1971).
[11] Oldridge et al., J. Phys. Chem. A, **115**, 2590-2598 (2011).

MISO: MORE THAN A JAPANESE SEASONING

J. Trachsel (ETHZ & WSL-SFL), M. Schneebeli (WSL-SFL), S. Avak (PSI & Univ. Bern), A. Eichler (PSI), J. Edebeli (PSI & ETHZ), T. Bartels-Rausch (PSI)

Microscale Distribution of Impurities in SnOw and Glacier Ice (MiSo) is a cross-disciplinary project of the Paul Scherrer Institute (PSI) and the WSL Institute for Snow and Avalanche Research (SLF). Its aim is to investigate the impact of metamorphism on impurity location in aging snow with detailed process studies in well-controlled laboratory based experiments.

Fig. 1 shows how drastically metamorphism shapes the structure and physical properties of snow, which has impacts on heat transfer, albedo, and avalanche formation. Such changes can be driven by water vapour fluxes in dry metamorphism with a mass turnover of as much as 60% per day - much greater than previously thought [1].

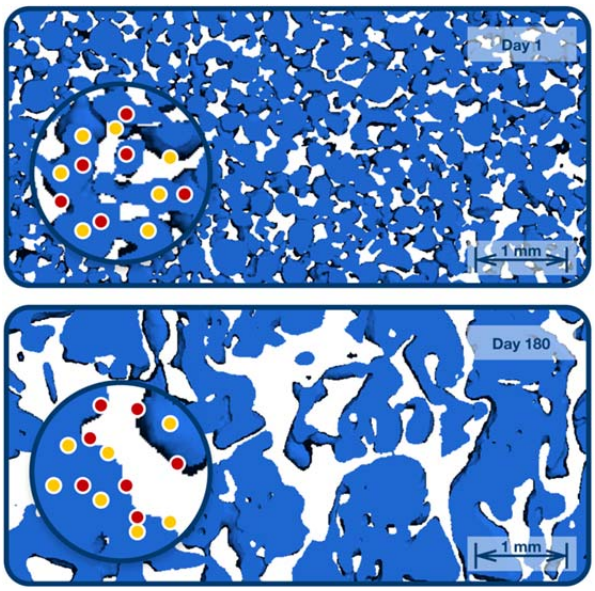

Fig. 1: Illustration of impurity relocation in snow during dry metamorphism. The pictures are visualisations of µCT scans showing the structural evolution of artificial snow with time.

The consequences for atmospheric science, snowphysics, and the ice core community are a current question of research [2]. Here, we focus on the fate of impurities during dry metamorphism. We propose that volatile impurities will follow the water vapour fluxes and will be incorporated into the growing ice based on their solubility while non-volatile species are left behind (Fig. 1). Fig. 2 shows a first result of a joint experiment to probe the segregation of impurities in ice crystals during snow metamorphism. For this, homogeneously doped artificial snow samples were produced, exposed to well-defined metamorphism conditions, and leached with 0°C water to determine the amount of impurities at the surface of the snow grains. The results of these elution experiments indicate a strong enrichment of some ions at the surface of snow crystals with time. The predominant exclusion of calcium and sulfate from the interior of the ice crystals and the embedding of the other species is in agreement with earlier observations in Alpine firn and roughly scales with solubility in ice [3].

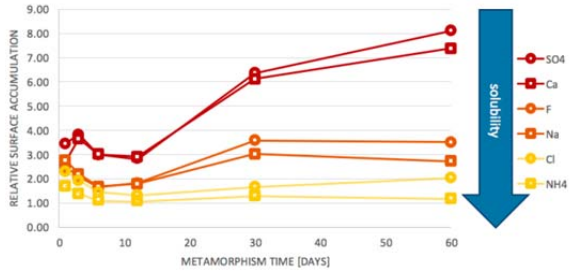

Fig. 2: Evolution of impurity enrichment at the crystal surface of artificial snow during metamorphism. The y-axis represents the concentration ratio after and before metamorphism.

These experiments confirm (a) that redistribution of impurities occurs and (b) the large differences among individual species. Furthermore, the structure of the artificial snow is indistinguishable from the natural snowcover [1].

Within MiSo, three parallel projects are running to investigate those processes in more detail:

- Kinetic experiments with such well-characterized, artificial snow will show to which extent the redistribution of impurities can explain the varying reactivity of snow with time;
- Isotopic measurements will better constrain the mass turnover rate;
- An analytical method to analyze the location of impurities with high spatial resolution is currently developed.

We acknowledge funding from the Swiss National Science Foundation (Grant 155999).

[1] B. Pinzer et al., The Cryosphere, **6**, 1141-1155, (2012).
[2] T. Bartels-Rausch et al., Atmos. Chem. Phys., **14**, 1587-1633 (2014).
[3] A. Eichler et al., Tellus, **53B**, 192-204 (2001).

https://www.psi.ch/luc/miso

TOWARDS A TOOL FOR LOCATING TRACE ELEMENTS IN GLACIER ICE

S. E. Avak (PSI & Univ. Bern), M. Birrer (PSI), M. Guillong, M. Wälle, O. Laurent (ETHZ), T. Bartels-Rausch (PSI), M. Schwikowski (PSI & Univ. Bern), A. Eichler (PSI)

Here, we report on the progress of the development of an analytical method, allowing investigation of the spatial location of trace elements in glacier ice.

Past changes in atmospheric pollution can be reconstructed from high-alpine ice core trace element records [1]. Percolation of meltwater alters the information originally stored in these environmental archives. Eichler et al. [2] suggested that the preservation of major ions with respect to meltwater percolation depends on their location in the crystal ice lattice. Major ions located at grain boundaries are prone to be removed by meltwater and tend to be depleted in the affected ice section whereas those incorporated into the ice interior are preserved and not disturbed. Other studies have also focused on the effect of meltwater on organic pollutant concentrations as well as on stable isotope profiles in ice cores, whereas no information exists about trace elements.

Within the Microscale Distribution of Impurities in SnOw and Glacier Ice (MiSo) project, we work towards a direct quantification of differences in concentrations of trace elements between grain boundaries and grain interiors in glacier ice. We use cryocell laser ablation inductively coupled plasma mass spectrometry (LA-ICP-MS), which is the method of choice for the direct *in situ* chemical analysis of trace elements at a sub-millimeter resolution in glacier ice [3, 4].

Following the construction of the cryocell [5] we searched for the optimal cooling medium. Ethanol has very good cooling properties and a low viscosity at low temperatures which is of advantage regarding the long and narrow channel system of the cryocell. However, due to its high volatility it diffused through the cooling tubes causing (even with the optimized flow pathway, see below) highly elevated background levels for many isotopes and various interferences typical for carbon. Silicon oil with its high creep capability caused exclusively an elevated long-lived background on *m/z* 28, which was unfavorable for the silicon measurements in geological samples performed by of our collaborators. Using a water/ethylene glycol mixture (2:3) turned out to be the best compromise between increased background and handling and obtaining a constant sample temperature of -25°C. Furthermore, we optimized the flow pathway of the carrier gas within the LA setup. Originally the carrier gas was supplied laterally into the ablation chamber, flushing the whole volume before taking up the ablated sample. To minimize the contact time between the carrier gas and the atmosphere in the chamber we designed a new ablation funnel. The carrier gas is now introduced as a ring curtain directly over the sampling spot to immediately take up the ablated sample. This adaption of the LA setup yielded in much lower carrier gas blanks. Moreover, we continued with the development of ice standards for calibration. The timespan between preparation and measurement of the ice standards needs to be as short as possible in order to prevent recrystallization processes which lead to a more inhomogeneous surface (Fig. 1). For the same reason the freezing temperature should be as low as possible. We implemented these two needs by shock freezing the standard solutions prior to their measurement by using liquid nitrogen. Currently we are comparing the effect of the freezing temperature and the acidity of the standard solutions on the outcome of the calibration (Fig. 2).

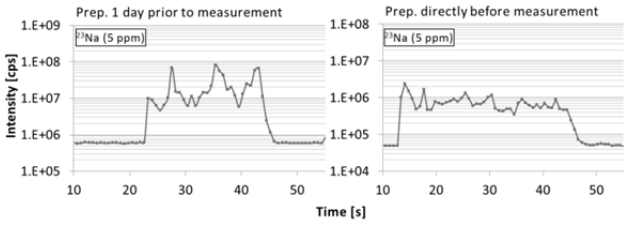

Fig. 1: LA signal comparison of two frozen standards differing in the timespan between preparation and measurement.

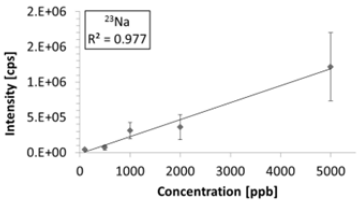

Fig. 2: Exemplary calibration curve for ^{23}Na.

As soon as the development of the calibration standards is finished we will use this new method to analyze trace element concentrations within grains and along grain boundaries in samples from both, unaffected sections of a high-alpine ice core and sections affected by an inflow of meltwater.

We acknowledge funding from the Swiss National Science Foundation (Grant 155999).

[1] M. Schwikowski et al., Environ. Sci. Technol., **38**, 957-964 (2004).
[2] A. Eichler et al., Tellus B, **53**, 192-204 (2001).
[3] S.B. Sneed et al., J. Glaciol., **61**, 233-242 (2015).
[4] D. Della Lunga et al., J. Glaciol., **60**, 970-988 (2014).
[5] S. E. Avak et al., Annual Report of the Lab. of Radio- & Environmen. Chem. PSI & Univ. Bern, p. 38 (2015).

A NEW METHOD TO QUANTIFY GLACIER ALBEDO REDUCTION BY IMPURITIES

A. Dal Farra (PSI & Univ. Bern), S. Kaspari (CWU), M. Schwikowski (PSI & Univ. Bern)

We use a hyperspectral imaging spectrometer to determine the optical properties of different light absorbing impurities, which reduce the surface albedo of glaciers.

Alpine glaciers are vital components of the earth's hydrological system. However, the current prevailing trend shows an increase in the rate of glacier retreat [1]. Previous studies have suggested that a decrease in surface albedo (the proportion of incident radiation that is reflected by a surface) plays a role in this phenomenon [2]. As example the decrease in surface albedo on Plaine Morte glacier is shown in Fig. 1.

Fig. 1: Plaine Morte glacier with fresh snow in June 2010 and a broadband albedo of 0.72 and in August 2015 with bare ice and a broadband albedo of 0.29.

The surface albedo of glaciers decreases with the presence of light absorbing impurities (LAI) [3] such as soot, mineral dust and humic substances. Soot has been investigated thoroughly in the climate science community as it is the only glacier LAI of anthropogenic origin and has a high mass absorption coefficient (MAC). Many studies also focus on the effect of LAI in snow whereas the albedo of snow free glacier surfaces has not had as much attention even though many glaciers are being subjected to snow free conditions in the warmest months. To comprehend the LAI's effect on the interaction between a glacier's bare surface and solar radiation it is necessary to understand their optical properties. Separating the LAI to measure their reflectance is a difficult process which can enhance the risk of altering their optical properties. Instead, we established a non-destructive method able to measure individually the reflectance spectra of all the different types of LAI present in the mixture without invasive sample treatment.

For this purpose we use a hyperspectral imaging spectrometer (HIS), which collects a hyperspectral image at 100x magnification in which every pixel (138 nm^2) of the image corresponds to a reflectrance spectrum, allowing us to measure the reflectance of very small particles. The use of this instrument is a novelty in the research concerning light absorbing impurities on glacier surfaces. The first step was to establish the analytical method. The standard setup of the instrument was modified by implementing a ring-light and rotating tray. Further, for this application a Spectralon reference is used to normalize the obtained spectra. To validate the method the spectra of a certain number of reference materials were collected with the HIS and compared with the spectra from a spectrometer that has been extensively used in LAI measurements (ASD Fieldspec 3) [4]. Reference materials included reflectance standards of 50% and 10% reflectance, a wavelength specific reflectance standard as well as a number of minerals, soot and organic materials. This comparison showed that the HIS captures valid reflectance spectra of the different types of materials. Soot, organic carbon and mineral particles were analyzed from an environmental sample collected on Plaine Morte glacier in summer 2015. The representative reflectance spectra indicate that organic matter has equally low reflectance as soot (Fig. 2).

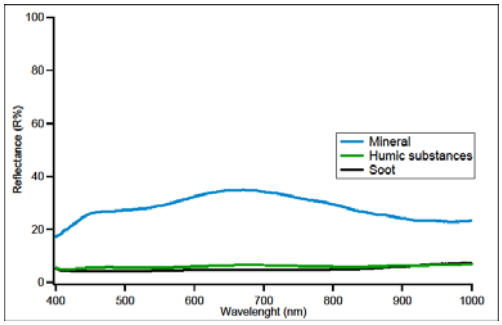

Fig. 2: Reflectance spectra of mineral dust, organic matter (humic substances) and soot (averages of 15 measurements).

Taking into account the average relative abundance of soot, mineral dust and humic substances on Plaine Morte glacier and their respective reflectance spectra we estimated that the contribution of mineral dust to the albedo reduction caused by LAI is dominant (87.7%), followed by organic matter (9.9%) and soot (2.5%).

We thank Thomas Bucheli from Agroscope for access to the HIS.
S. Kaspari acknowledges funding from the Swiss National Science Foundation (IZK0Z2_160953).

[1] M. Zemp et al., J. Glaciol. **61,** 745-761 (2015).
[2] S.G. Warren and W.J. Wiscombe, J. Atmos. Sci., **37,** 10.1175/1520-0469(1980)037 (1980).
[3] S. Kaspari et al., J. Geophys. Res-Atmos., **120,** 7, 2793-2807 (2015).
[4] K. Naegeli et al., Remote Sens. Environ. **168,** 388-402 (2015).

FIRE ACTIVITY AND CLIMATE IN CENTRAL ASIA

M. Sigl (PSI), D. Osmont, P.-A. Herren (PSI & Univ. Bern), S. Brügger (Univ. Bern/IPS), T. Papina (IWEP), M. Schwikowski (PSI & Univ. Bern)

We discuss trends of ice-core indicated fire activity and temperatures in Central Asia in relation to external climate forcing from solar and volcanic activity. Over the past centuries, forest fire frequency closely followed solar activity, while volcanic eruptions frequently triggered cooling extremes.

Devastaing, uncontrolled fires have increasingly occurred in recent years, resulting in enormous economic costs and disruption of habitats. Air pollution plumes related to extreme fire events are of growing concern due to their effect on human health [1]. Nevertheless the drivers for longterm biomass burning are still debated. The aim of our record situated in the Mongolian steppes is a long term assessment of vegetation response to climatic changes, societal impacts and fire disturbances over the past six millennia.

Here we present first measurements of black carbon performed on the 72 m long Tsambagarav ice core (Mongolian Altai, [2]) spanning 1620 to 1950 AD using a SP2 single particle soot photometer. Sampled at annual to sub-annual resolution, this precisely dated record reflects the changes of large-scale fire activity in Central Asia over the past centuries. In tandem with glaciochemical (mineral dust, stable isotopes) and biological (pollen assemblages, micro-charcoal) climate tracers this will enable reconstruction of past climate, fire activity and land-use changes covering the past 6,000 years.

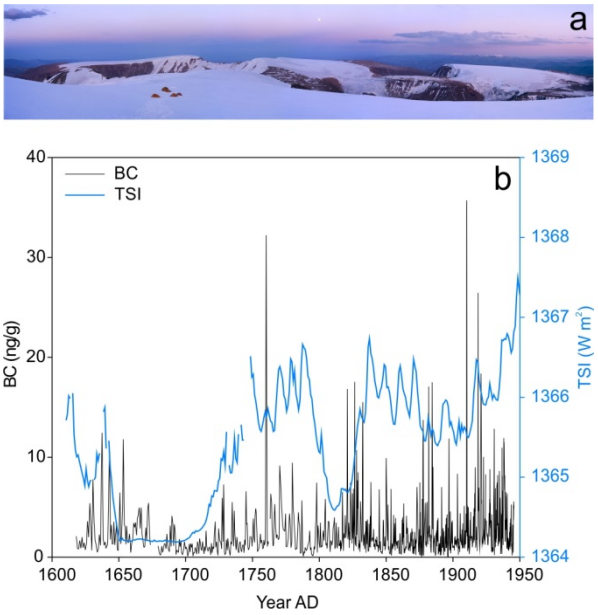

Fig. 1: a) View of the study site; b) ice-core black carbon (BC) concentration record from 1620-1945 AD and reconstructed total solar irradiance (TSI) [3].

BC concentrations are log-normally distributed with median concentrations as low as 2 ng/g (Fig. 1). Distinctive biomass burning episodes from natural or anthropogenic sources can be identified using an outlier detection algorithm. Between 1750-1900 AD a total of 39 individual burning events are registered, which is approximatly twice as many (per century) as are observed for the Colle Gnifetti ice core in the European Alps during the preindustrial, indicating a larger frequency of natural fires in the Siberian boreal forest upwind of this continental site. A distinct reduction of fire activity is evident between 1660 and 1720 AD, coincident with a period of reduced solar activity ("Maunder Minimum") and generally lower summer temperatures in the Altai [4] which potentially surpressed fuel growth and ignition.

Cold summer temperature extremes in Central Asia are frequently caused by volcanic sulphate emissions [4, 5]. This is evident also for the Tsambagarav ice-core (Fig. 2), which shows significant reductions in $\delta^{18}O$ following most of the largest eruptions since 1800 AD. Combined, these first results illuminate a strong sensitivity of both temperatures and fire activity to external climate forcings, likely explained by the continentality of the climate and the remoteness of the study site away from major human population centres.

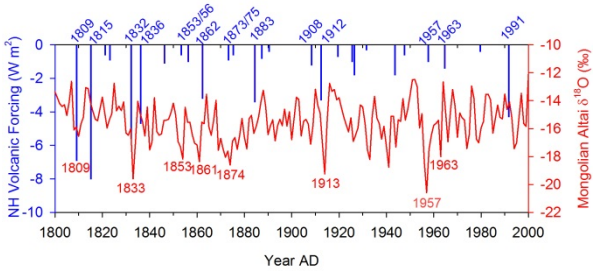

Fig. 2: Ice-core $\delta^{18}O$ record from 1800-2000 AD, and reconstructed Northern Hemisphere volcanic forcing [5]. Cold years and major volcanic eruptions are indicated.

We acknowledge funding from the Swiss National Science Foundation (Sinergia: Paleo fires from high-alpine ice cores 154450).

[1] M. A. Moritz et al., Nature, **515**, 58-66 (2014).
[2] P. A. Herren et al., Quat. Sci.. Rev., **69**, 59-68 (2013).
[3] J. Lean et al., Geophys. Res. Lett. **22**, 3195-3198 (1995).
[4] U. Büntgen et al., Nature Geosc. **9**, 231-236 (2016).
[5] M. Sigl et al., Nature, **523**, 543-549 (2015).

PALEOFIRES RECORDED IN THE LOMONOSOVFONNA ICE CORE, SVALBARD

D. Osmont, L. Schmidely, I. Wendl (PSI & Univ. Bern), M. Sigl, T. M. Jenk (PSI), E. Isaksson (NPI), M. Grieman (UCI), M. Schwikowski (PSI & Univ. Bern)

A 800-year record of different fire tracers shows that forest fire activity did not change significantly over the preindustrial times.

Ice cores retrieved from polar and high-mountain glaciers are a powerful tool to reconstruct paleoclimates due to the fact that glaciers behave as natural archives by trapping chemical information from the atmosphere. Our inter-disciplinary Paleo Fire project aims to better understand the complex relationship between humans, fire and climate, and to test the "broken fire hockey stick" hypothesis [1], a decoupling between fire activity and its main drivers (temperature and population density) since 1870, by reconstructing regional paleofire history from high-mountain ice cores for the last 2000 years.

In this work, four forest fire proxies with different specificities have been combined. Two of them are not specific for forest fires because they can be emitted by other sources: black carbon (BC), which is produced by the incomplete combustion of fossil fuels and biofuels from both anthropogenic and natural origin including wildfires [2], and ammonium (NH_4^+), not only reflecting forest fires but also biogenic and agricultural emissions. However, vanillic acid (VA) and p-hydroxybenzoic acid (HBA) are only emitted by biomass burning. BC was analyzed with a Single Particle Soot Photometer (SP2) according to the protocol given by [3], NH_4^+ by ion chromatography and VA and HBA using liquid chromatography coupled to mass spectrometry. In fig. 1, we present our multi-proxy record from the well-dated Lomonosovfonna ice core, drilled in Svalbard in 2009, which spans the last 800 years.

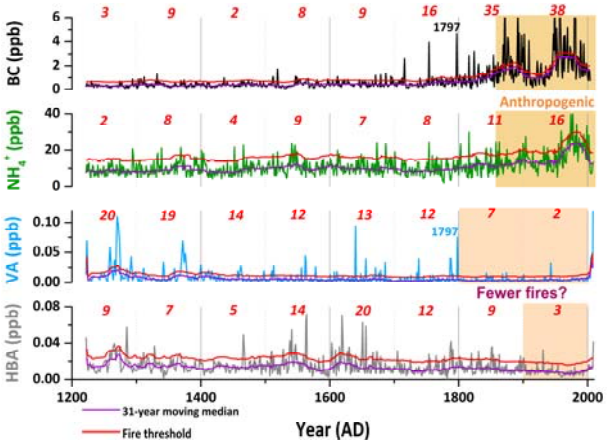

Fig. 1: BC, NH_4^+, VA and HBA annual averages in the Lomonosovfonna core along with 31-yr moving medians and associated fire threshold. Red numbers represent the number of years per century above the fire threshold.

From the annual averages, the 31-year moving medians have been calculated, and a fire threshold has been defined as the median plus three times the median absolute deviation, according to [4]. Every annual average above this threshold can thus be considered as a year with significant biomass burning emissions, and finally the centennial frequency of such events can be obtained.

It is interesting to note that the different proxies show different behaviours regarding fire frequencies because they can reflect different conditions in terms of emission, transport and deposition. However, all in all, the forest fire frequency did not change significantly over preindustrial times. A downward trend throughout the Little Ice Age due to decreasing temperatures is not visible in our record. The 1797 peak is of particular interest because it has also been detected in several ice cores from Greenland.

From 1800 onwards, the concentrations of the non-specific proxies started to rise due to increasing anthropogenic input induced by the Industrial Revolution. They strongly correlate with nitrate and sulfate which are proxies for traffic/energy production and fossil fuel combustion, respectively. After 1860, the anthropogenic influence overwhelmed the signal in such a way that forest fire detection was no longer possible with those proxies. However, those tracers kept track of interesting features reflecting historical trends. Nevertheless, both the mismatch with emission estimates and the early 20th century BC trough reveal that the record is disturbed by melting in its uppermost part, which is in agreement with the melt index.

Still, the forest fire detection can be achieved in the industrial times using VA and HBA. Both clearly show a decrease in the forest fire frequency, which could support the broken fire hockey stick hypothesis. Although the behaviour of the different fire tracers has not been extensively compared so far, our study shows that it is crucial to use several proxies with different specificities in order to get a comprehensive overview of the situation.

We acknowledge funding from the Swiss National Science Foundation (Sinergia: Paleo fires from high-alpine ice cores 154450).

[1] J. R. Marlon et al., NGEO., **1**, 697-702 (2008).
[2] T. C. Bond et al., J. Geophys. Res.-Atmos., **118**, 5380-5552 (2013).
[3] I. A. Wendl et al., Atmos. Meas. Tech., **7**, 2667-2681 (2014).
[4] H. Fischer et al., NGEO., **8**, 723-727 (2015).

ALTAI ICE CORE REVEALS BIOSPHERE DYNAMICS DURING 5500 YEARS

S. O. Brügger, E. Gobet (Univ. Bern/IPS), M. Sigl, D. Osmont (PSI), M. Schwikowski (PSI & Univ. Bern), T. Papina (IWEP), W. Tinner (Univ. Bern/IPS)

Using a continuous palynological ice-core record spanning the past 5 millennia we reconstruct the longterm fire and vegetation dynamics including land use for the steppic environments of Western Mongolia.

Devastating, uncontrolled fires have increasingly occurred in recent years, resulting in enormous economic costs and disruption of habitats [1], but the drivers and environmental effects of long-term biomass burning are still debated.

Our high-alpine ice core (4130 m a.s.l.) was collected at Tsambagarav Mountain in the Mongolian Altai. A sound chronology was developed on the basis of ^{14}C-dates and absolute time markers e. g. volcanic eruptions, which is excellent during the past 200 years [2]. We use pollen and spores as proxies for past vegetation changes and land use activity, microscopic charcoal (>10 µm) as a proxy for regional fire activity, and spheroidal carbonaceous particles (SCP) as a proxy for fossil fuel combustion [3].

The pollen record is dominated by pollen of the steppic herbaceous taxa *Artemisia* (ranging from 20 to 90%) with continuous presence of various arboreal pollen, e.g. *Betula, Pinus sibirica, Corylus* indicating the dominance of steppic vegetation with isolated woodlands in the catchment. *Sporormiella*, a coprophilous fungal spore, suggests conspicuous grazing activities since the beginning of the record 5500 years ago. The arboreal pollen percentage curve suggests a marked expansion of woodlands between 3200 BC and 1900 BC with two brief forest reduction phases of which the latter is coeval with a century-long drought spell at 4.2 k yr [4]. The forest vegetation declined permanently at 1900 BC and steppes re-expanded (e. g. increase of *Artemisia* pollen). The record suggests a further decline of forested areas at ca. 1100 AD. 100 years later Dshingis Khan's empire rose around 1200 AD. Even if antecedent, we speculate that environmental changes (drought, reduction of vegetation) may have contributed to societal instability such as the Mongolian invasions in Eurasia [5,6].

The charcoal record suggests no marked trend in fire activity until 1700 AD (c. 5000 part./l) with a single charcoal peak around 1600 BC (30'000 part./l). Fire activity was low during the past 300 years which coincides with a third woodland decline after 1700 AD. SCPs start to be accumulated in the ice after 1720 AD except for one early particle at ca. 3300 BC, possibly a contamination. SCPs increase pronouncedly after 1950 AD, a shift which is also recorded in the Alpine Colle Gnifetti record, although with 10x higher concentrations there (2000 vs. 150 part./l). This finding mirrors the globally observed increase of SCP in lake sediments, which is related to the intensified fossil fuel burnings over the last decades [7].

Our results reveal significant and repeated woodland expansions in the Mongolian steppes 3200-1900 BC. The most likely cause is oscillations of moisture, the forest limiting factor in the region. The charcoal record suggests the lack of any pronounced fire activity trend during the late Holocene. Burning probably reached a minimum at the onset of the industrial period. Common initial SCP signals in Europe and Central Asia during the 18th century suggest a surprisingly early onset of pollution in Eurasia.

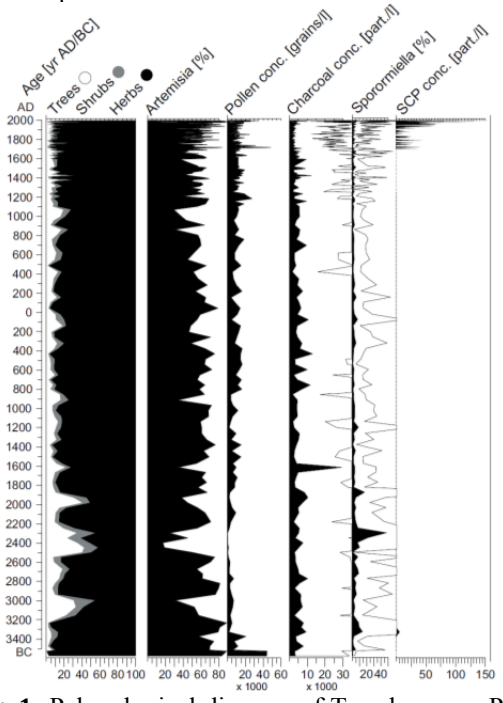

Fig. 1: Palynological diagram of Tsambagarav. Pollen and *Sporormiella* percentages are based on a pollen sum including trees, shrubs and terrestrial herbs. Charcoal and SCP concentrations were assessed by adding exotic markers (*Lycopodium*) to the melted ice samples. White curves show 10 x magnifications.

We acknowledge funding from the Swiss National Science Foundation (Sinergia 154450).

[1] M. A. Moritz et al., Nature, **515**, 58-66 (2014).
[2] P. A. Herren et al., Quat. Sci. Rev., **69,** 59-68 (2013).
[3] A. Eichler et al., Quat. Sci. Rev., **30**, 1027-1034 (2011).
[4] T. J. Szczęsny, OJE **6**, 613-631 (2016).
[5] N. Pederson, PNAS, **111**, 4375-4379 (2014).
[6] J. Pongratz, Holocene, **21**, 843-851 (2011).
[7] N. L. Rose, Environ. Sci. Technol., **49**, 4155-4162 (2015).

HOW CLOUDY WAS THE PRE-INDUSTRIAL ATMOSPHERE?

A. L. Vogel, K. Dällenbach, I. El-Haddad, I. Wendl, A. Eichler, S. Brütsch (PSI), M. Schwikowski (PSI & Univ. Bern)

Here, we present a new approach for the chemical characterization of the organic fraction preserved in high alpine ice cores to reconstruct trends of atmospheric organic aerosols. They will allow new insights on organic aerosol composition and mass in the pre-industrial atmosphere, which can help to improve climate models trough evaluation of our current understanding of aerosol radiative effects.

Atmospheric aerosols are liquid or solid particles suspended in the air, providing surface for water condensation, thus playing a key role as cloud condensation nuclei (CCN) in the climate system [1]. Recent studies showed that atmospheric oxidation of biogenic volatile organic compounds (BVOCs) leads to the production of highly oxidized organic compounds, which can nucleate new particles in the atmosphere without sulfuric acid being involved [2, 3]. This mechanism increases the prediction of the natural pre-industrial aerosol number in global climate models, and thus the reflectivity of clouds and cloud-lifetime, which results in a net decrease of the previously estimated negative forcing effect of anthropogenic aerosols [4]. This highlights the need for the evaluation of such model outcomes by directly analyzing organic aerosol particles from the pre-industrial atmosphere, which are preserved in ice cores. Previous studies, which aimed to characterize the organic fraction in ice, have examined low-molecular weight organic acids and extractable non-polar compounds, while historic trends of water-soluble higher-molecular weight compounds, which in sum comprise the majority of organic carbon in ice, have rarely been reported [5].

Using a combination of quantitative electron ionization (EI) and qualitative chemical ionization techniques coupled to time-of-flight and fourier-transform mass spectrometry, respectively, we plan to retrieve quantitative historic trends of the total organic mass, classified into groups of different sources or formation pathways and underpinned by specific molecular markers. Measurements of the major ions by ion chromatography (IC) will help to evaluate the method.
In a proof-of-principal study we analyzed an 800 year ice core record from the Lomonosovfonna glacier ice core, drilled in 2009 in Svalbard, Norway, using a setup that has until then only been applied on offline measurements of aerosol filter extracts [6]. The melted ice was nebulized and dried, such that aerosols are formed from the soluble and insoluble organic and inorganic compounds that are preserved in the ice. To improve the sensitivity, the aerosol stream was then enriched by the application of an online aerosol concentrator, before the aerosol was analyzed by EI within a high resolution time-of-flight aerosol mass spectrometer (HR-ToF-AMS). We were able to demonstrate that this setup is a quantitative method toward nitrate and sulfate when internal inorganic standards of $NH_4{}^{15}NO_3$ and $(NH_4)_2{}^{34}SO_4$ are added to the sample. Comparison between AMS and IC measurements of nitrate and sulfate resulted in a good agreement (Fig. 1). The organic fraction, however, was biased by a source of organic contamination, likely introduced during sample storage. Freshly prepared ice blanks showed no significant source or organics, and the calibration with an organic surrogate standard demonstrated that this technique is applicable for the analysis of fresh ice samples.

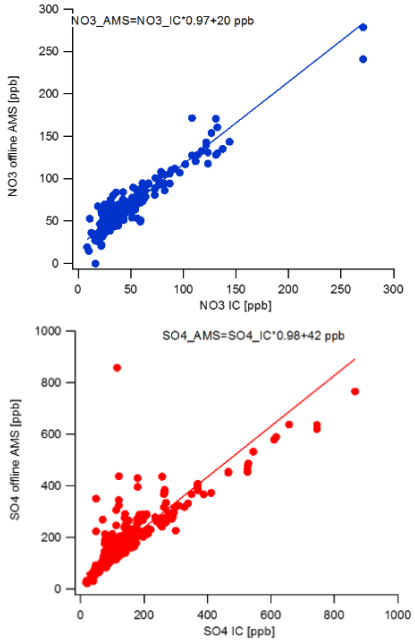

Fig. 1: Concentrations of nitrate and sulfate in the Lomonosovfonna ice core, analysed with the offline AMS method and IC, respectively. Overprediction of AMS sulfate likely originates from the presence of methanesulfonic acid or other organic sulfate species preserved in the ice.

We acknowledge funding from the PSI-CROSS Project *"Reconstruction of long-term organic aerosol concentrations from glacier ice cores"*.

[1] O. Boucher et al., IPCC 5th Assessment Report, (2013).
[2] J. Kirkby et al., Nature, **533**, 521-526 (2016).
[3] F. Bianchi et al., Science, **352**, 1109-1112 (2016).
[4] H. Gordon et al., Proc. Nat. Acad. Sci., **113**, 12053-12058 (2016).
[5] M. Legrand et al., Clim. Past, **9**, 2195-2211 (2013).
[6] K. Dällenbach et al., Atmos. Meas. Tech., **9**, 23-39 (2016).

RADIOCARBON DATING OF GLACIER ICE

C. Uglietti (PSI & Univ. Bern), A. Zapf (PSI & Univ. Bern, deceased), T. M. Jenk, M. Sigl (PSI), S. Szidat, G. Salazar (Univ. Bern), M. Schwikowski (PSI & Univ. Bern)

A precise chronology is crucial for a meaningful interpretation of the valuable past climatic signals contained in high-altitude glaciers from mid-latitudes and tropical regions. Here the potential of radiocarbon dating of the water-insoluble organic carbon contained in the ice for establishing such chronologies is discussed.

For dating the upper part of ice cores from such sites, several relatively precise methods exist, but they fail in the older and deeper parts, where plastic deformation of the ice results in strong annual layer thinning and in a non-linear age–depth relationship.

If sufficient organic matter such as plant, wood or insect fragments were found, radiocarbon (^{14}C) analysis would be the only option for a direct and absolute dating of the deeper ice core sections. However, such fragments are rarely found at the desired depth and resolution. About 10 years ago, a new, complementary dating tool was therefore introduced by our group. It is based on extracting the µg-amounts of the water-insoluble organic carbon (WIOC) fraction of carbonaceous aerosols embedded in the ice matrix for subsequent ^{14}C dating [1]. Since then this new approach has been improved considerably by reducing the measurement time and improving the overall precision. Samples with ca. 10 µg WIOC mass can now be dated with reasonable uncertainty of around 10–20%. This requires about 300 to 800 g of ice for WIOC concentrations typically found in mid-latitude and low-latitude glacier ice. The accuracy of the method was validated by applying this method to independently dated ice, see Fig. 1.

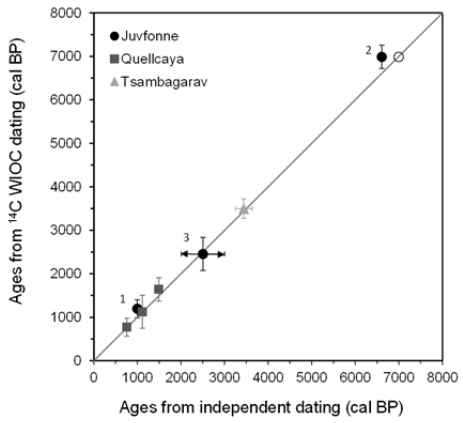

Fig. 1: Scatter plot showing ages obtained with WIOC ^{14}C for independently dated ice, including conventional ^{14}C dates (Juvfonne organic-rich layers [2]), a dated fly in the Tsambagarav ice core [3] and the annual layer counting dated Quelccaya ice [4]. Error bars denote the 1σ uncertainty. For more details see [2, 5].

With this method, the deepest parts of the ice cores from Colle Gnifetti [6] and the Mt Ortles glacier [7] in the European Alps, Illimani glacier in the Bolivian Andes [8], Tsambagarav ice cap in the Mongolian Altai [3], and Belukha glacier in the Siberian Altai [9] have been dated. In all cases a strong annual layer thinning towards the bedrock was observed and the oldest ages obtained were in the range of 10,000 years. WIOC ^{14}C dating was not only crucial for interpretation of the embedded environmental and climatic histories, but additionally gave a better insight into glacier flow dynamics close to the bedrock and past glacier coverage. The strength of the WIOC ^{14}C dating method is the potential to determine absolute ages from principally every piece of ice.

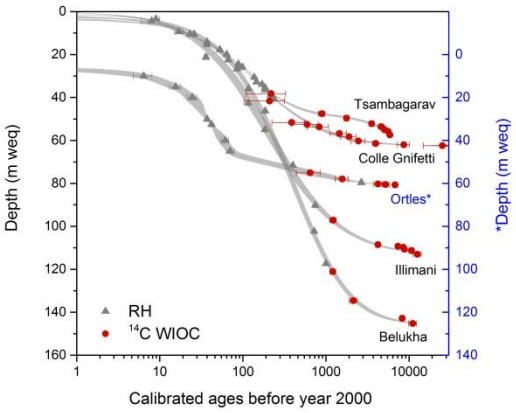

Fig. 2: Compilation of age–depth relationships for five different ice cores, highlighting the importance of the WIOC ^{14}C dating for obtaining continuous chronologies. RH: Reference Horizons.

We acknowledge funding from the Swiss National Science Foundation (Grant 200020_144388) and from the Oeschger Centre for Climate Change Research of the University of Bern.

[1] T. M. Jenk, et al., NIMB, **259**, 518-525 (2007).
[2] Ødegård et al., The Cryosphere, **11**, 17-32 (2016).
[3] P. A. Herren et al., Quat. Sci. Rev., **69**, 59-68 (2013).
[4] L. G. Thompson et al., Science, **340,** 945-950 (2013).
[5] C. Uglietti et al., The Cryosphere, **10**, 3091-3105 (2016).
[6] T. M. Jenk, et al., J. Geophys. Res., **114** (2009).
[7] P. Gabrielli, et al., The Cryosphere, **10**, 2779-2797 (2016).
[8] M. Sigl et al., J. Glaciol., **55**, 985-996 (2009).
[9] E. Aizen et al., J. Glaciol., **62**, 1-29 (2016).

DATING OF AN ICE CORE FROM CHONGCE ICE CAP, CHINA

C. Wang (PSI & Univ. Nanjing), T. M. Jenk, S. Köchli (PSI), C. Uglietti (PSI & Univ. Bern), J. Eikenberg (PSI), E. Vogel, S. Szidat (Univ. Bern), S. Hou (Univ. Nanjing), M. Schwikowski (PSI & Univ. Bern)

^{3}H, ^{210}Pb and ^{14}C dating of the Chongce ice core consistenly suggest a mean net accumulation rate of 28 cm w.e., higher than at nearby Guliya glacier. Accordingly, the age of the ice close to bedrock is only a few thousand years, much younger than anticipated.

Mid- or low-latitude glaciers represent natural archives, well suited for studying past environmental and climatic conditions on the regional scale. The West Kunlun Mountains has been shown to be a potential place for obtaining the oldest ice core record in the Tibetan Plateau [1]. In October 2013, a 216.6 m ice core was drilled to bedrock from Chongce ice cap in this mountain range (35º14′ 56.58″ N, 81º5′ 27.7″ E, 6105 m a.s.l) (Fig. 1). Accurate dating is an essential prerequisite for the interpretation of paleoclimatic information from ice core records. For the time period covered by ice cores, ranging from decades to thousands of years, different radioisotope dating methods have been used for obtaining chronologies [2, 3, 4]. In this work, ^{3}H, ^{210}Pb and ^{14}C dating methods were applied to establish the age-depth relationship of the 216.6 m ice core from Chongce ice cap.

Ice core sectioning was performed in the cold room of the Nanjing University and PSI at -20°C. ^{3}H activity was measured by β-liquid scintillation counting and ^{210}Pb activity by α-spectroscopy [3] at PSI. 19 samples were prepared for ^{14}C analysis of the water-insoluble organic carbon (WIOC) fraction of carbonaceous embedded in the ice matrix, according to the procedure decribed in [4, 5, 6]. ^{14}C was measured with the Mini Carbon Dating System (MICADAS) at the LARA laboratory, University of Bern. Conventional ^{14}C ages were calibrated using OxCal v4.2.4 software with the IntCal13 calibration curve [7, 8].

The ^{3}H peak from nuclear test fallout with an activity of 3237±89 Tritium Units (TU, decay corrected to the year 1963) was detected at a depth of 15.1 m w.e. The high ^{210}Pb surface activity at the Chongce ice cap of 236±33 mBq/kg allowed dating back to 1891±15 AD. The ^{210}Pb dating is consistent with the ^{3}H peak. The ^{14}C ages indicate an overall increase with depth, but also a lot of scattering in the 90 m w.e. to 140 m w.e. depth range. Generally, the ice close to bedrock is much younger than anticipated, consistent with a relatively high annual net accumulation rate of 28 cm w.e. compared to what was obtained for nearby Guliya ice cap (20 cm w.e. [1]). To establish a continous age-depth relation for the whole ice core, a two parameter model was applied [9] [Fig. 2]. The 1σ-uncertainty range is relatively broad, where the ^{14}C ages scatter (22.8-177.3 m w.e.). This scatter is possibly caused by a high dust content of the ice, resulting in incomplete removal of carbonates during WIOC extraction.

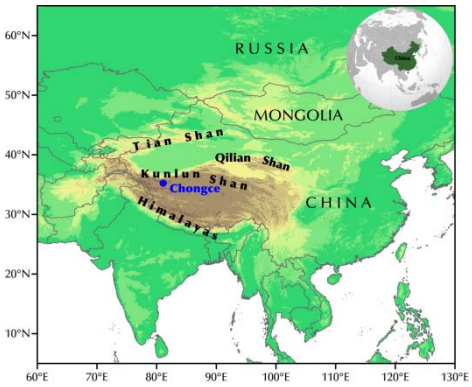

Fig. 1: Location of the Chongce ice core drilling site.

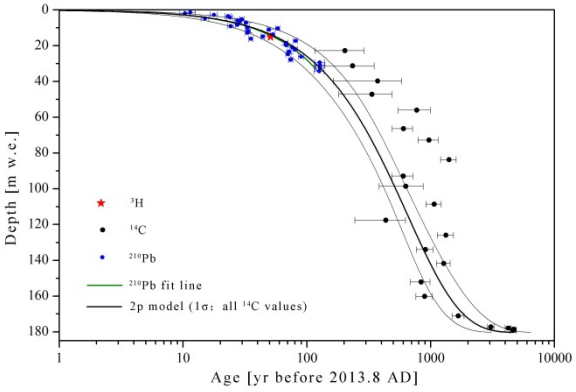

Fig. 2: Age-depth relationship for the Chongce ice core. ^{210}Pb activity (blue dots), ^{210}Pb age fit (green line), tritium peak (red star), ^{14}C values with 1σ-range (black dots), and 2p glacier flow model fit with 1σ confidence band (solid gray line).

This work was supported by the Swiss Government Excellence Scholarship granted to Wang Chaomin, PhD student at Nanjing University.

[1] L. Thompson et al., Science, **276**, 1821-1825 (1997).
[2] A. Eichler et al., J. Glaciol., **46**, 507-515 (2000).
[3] H. W. Gäggeler et al., J. Glaciol., **29**, 165-177 (1983).
[4] T. Jenk et al., J. Geophys. Res., **114**, D14 (2009).
[5] M. Sigl et al., J. Glaciology., **55**, 985-996 (2009).
[6] C. Uglietti et al. The Cryosphere **10**, 3091-3105 (2016).
[7] B. Ramsey et al., Radiocarbon, **55**, 2-3 (2013).
[8] P. J. Reimer, et al., Radiocarbon, **55**, 1869-1887 (2013).
[9] L. Thompson et al., Ann. Glaciol., **14**, 288-297 (1990).

EXTRACTION OF DISSOLVED ORGANIC CARBON FOR RADIOCARBON DATING

L. Fang, J. Schindler (PSI & Univ. Bern), T. M. Jenk (PSI), M. Schwikowski (PSI & Univ. Bern)

Recent improvements of the radiocarbon analysis technique allow us to develop a new ice dating method based on dissolved organic carbon (DOC) in glacier ice. Two critical characteristics (blank and oxidation efficiency) of the DOC extraction setup were investigated.

A precise age-depth relationship in ice cores is essential for paleoclimate studies. However, the study of mid-latitudes and tropical mountain glaciers' age-depth relationship in the deeper part is limited by a lack of dating techniques due to complex bedrock geometry and strong annual layer thinning. This project is mainly aimed at developing a radiocarbon dating method using DOC in ice cores to reconstruct the glacier chronological context. Radiocarbon dating of water insoluble organic carbon (WIOC) was proposed as a dating tool to constrain the age of ice from nonpolar glaciers about 10 years ago and the accuracy of this method has been validated recently [1]. However, in some cases this method is restricted by the low WIOC concentrations (10-60 ppb) present in the ice [2]. Considering the relatively higher concentrations of DOC (50-100 ppb) [3], radiocarbon dating of DOC demand less ice volume and may allow dating even when the WIOC concentration is too low.

The extraction method, in brief, after cutting and cleaning of ice samples in the cold room at -20°C, samples are melted and further cleaned under helium inert gas conditions in a melting vessel. WIOC is separated by filtration and inorganic carbon (IC) is removed via acidifying and degassing with helium. The remaining DOC in the solution is oxidized by two UV lamps in a quartz glass photo-reactor. Then produced CO_2 is collected by cryogenic traps and further cleaned, quantified and sampled to glass vials for ^{14}C analyses [4]. The radiocarbon analyses will be conducted at the MICADAS AMS equipped with a gas inlet system of the LARA laboratory, Department of Chemistry and Biochemistry of the University of Bern.

The oxidation process results in a blank of 1.7 ± 0.9 µgC (n=3), which is determined through irradiation of ultra-pure water (UPW) in the pre-cleaned system. The total blank (including ice cutting, filtration and oxidation) is slightly higher with about 2.4 ± 1.2 µgC (n=3) using UPW ice. At 45 min irradiation time, we found average oxidation efficiencies of 82%, 105%, 79% and 54% for oxalate, formate, phthalate and acetate, respectively. The time required for 70% recovery rate of 100 µg carbon varies from about 25 min to 120 min (extrapolated) for the different substances (Fig.1). Preliminary results also suggest higher oxidation efficiencies for longer irradiation time.

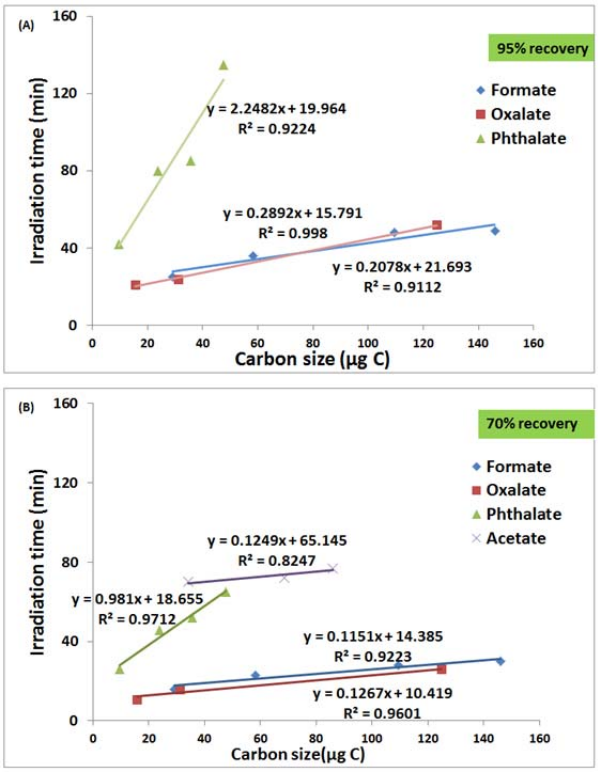

Fig. 1: Irradiation time of different compounds. (A) The estimated time at 95% recovery. (B) Irradiation time for a 70% recovery.

We applied this extraction method to snow samples which were collected from Ewigschneefeld in 2012. With an irradiation time of 45 min, a DOC concentration of 87 ± 3 ppb was obtained. However, at a longer irradiation time of 90 min the DOC concentration was slightly higher (120 ± 2 ppb). In order to determine the optimal irradiation time for high oxidation efficiency and low blank, more snow and ice samples will be processed in future. Next year we will focus on the radiocarbon determination in various snow and ice samples to address the anthropogenic contribution to glacier DOC and to establish the time boundary of applying this radiocarbon analysis as a dating tool.

We acknowledge support from M. Birrer.

[1] C. Uglietti et al., The Cryosphere, **10**, 3091-3105 (2016).
[2] T. M. Jenk et al., J. Geophys. Res., **114**, D14305 (2009).
[3] M. Legrand et al., J.Geophys. Res., **118,** 3879-3890 (2013).
[4] J. Schindler, PhD thesis Univ. Bern, in preparation.

RADIOCARBON DATING OF AN ARCHEOLOGICALLY SIGNIFICANT ICE PATCH

C. Uglietti, M. Schwikowski (PSI & Univ. Bern), R. S. Ødegård (NTNU), A. Nesje (UiB)

Despite numerous spectacular archaeological discoveries worldwide related to melting ice patches and the emerging field of glacial archaeology, the governing processes related to ice patch development during the Holocene and their sensitivity to climate change are still largely unexplored.

New results from an extensive 6-year (2009 – 2015) field experiment at Juvfonne, a small perennial ice patch in Jotunheimen, central southern Norway (61.68° N, 8.35° E) are presented. Radiocarbon dating performed by means of accelerator mass spectrometry (AMS) of organic-rich layers and of water insoluble organic carbon aerosols (WIOC) embedded in the clear ice is discussed. The results show that the Juvfonne ice patch has existed continuously since the late Mesolithic period.

In addition to the 30 m long ice tunnel opened in May 2010 in the Juvfonne ice patch, a new 70 m long tunnel was excavated into the central parts of the ice patch in spring 2012. The tunnels were cut with specially designed ice axes, causing minimal disturbance to the surrounding ice. The tunnels gave an excellent opportunity to collect organic material and ice for radiocarbon dating [2, 3, 4].

Two samples of clear ice adjacent to the organic-rich layers and a surface sample were collected in the 2010 tunnel. The results derived using WIOC agreed well with the corresponding conventionally dated ^{14}C ages, ranging between modern age in the top layer at the entrance and ages ranging from 3065-3174 to 963-1052 cal years BP inside the tunnel. These results were previously published [3] and recalibrated [2].

In autumn 2014, two in situ *Polytrichum* moss mats melted out along the margin of Juvfonne south of the ice tunnel excavated in 2010. ^{14}C ages of the two moss mats indicate that the moss was killed by the expanding margin of the ice patch about 2000 years ago. Thus, the minimum extent of the south-eastern part of the ice patch observed in September 2014 is most likely the smallest in 2000 years.

In summer 2015 additional clear ice samples were collected adjacent to a conventionally ^{14}C dated plant fragment found in an organic-rich layer at the base of the 2012 tunnel [2, 4]. Four ice blocks were collected and subdivided into two subsamples each. Ice block 1 (JUV 0_A) was taken adjacent to the plant fragment layer, ice block 2, ice block 3 and ice block 4 (JUV 0_B) at the bottom of the wall, a few centimetres below the plant fragment layer. JUV 0_A yielded an average age of 6966±264 cal BP, in good agreement with the age of the plant fragment layer of 6595±47 cal BP, considering the observed increase in age with increasing depth. The average age of the other three blocks (JUV 0_B) is 7476–7785 cal years BP.

In general, the ages obtained from dating of carbonaceous aerosol particles in the ice are and of the organic debris are consistent [2]. In Fig. 1 ^{14}C ages from both ice tunnels are plotted according to their vertical distance from bed.

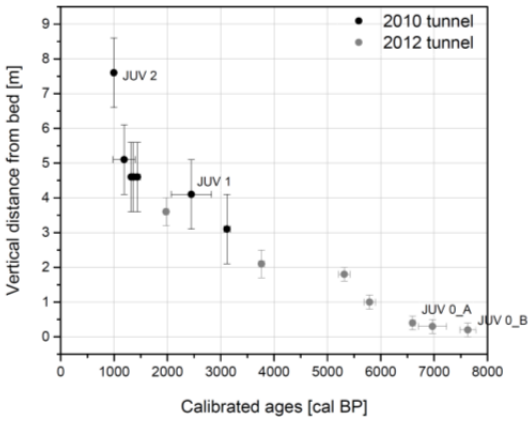

Fig. 1: ^{14}C ages of clear ice samples and organic remains from the two ice tunnels.

During the study period, the mass balance record showed a strong negative balance, and the annual balance is highly asymmetric over short distances. Snow accumulation is poorly correlated with estimated winter precipitation, and single storm events may contribute significantly to the total winter balance. There is sufficient meltwater to bring the permeable snowpack to an isothermal state within a few weeks in early summer [2].

The exploratory study of Juvfonne gives new insights into age, internal structure, mass balance and climate sensitivity of this small ice patch. ^{14}C ages range from modern at the surface to ca. 7600 cal years BP at the bottom, thus implying that Juvfonne has existed continuously during the last 7600 years. This is the oldest dating of ice in mainland Norway.

We acknowledge funding from the Swiss National Science Foundation (Grant 200020_144388) and by the Oeschger Centre for Climate Change Research of the University of Bern.

[1] A. Nesje et al., The Holocene, **22**, 485-96 (2012).
[2] R. S. Ødegård et al., The Cryosphere, **11**, 17-32 (2017).
[3] A. Zapf et al., Radiocarbon, **55**, 571-578 (2013).
[4] C. Uglietti et al., The Cryosphere, **10**, 3091-3105 (2016).

CONSTRAINING THE DEPTH-AGE SCALE OF A TEMPERATE GLACIER

S. Kaspari (CWU), T. Jenk (PSI), D. Pittenger (CWU), U. Morgenstern (GNS), N. Buenning (USC), M. Schwikowski (PSI & Univ. Bern)

This study demonstrates the difficulty in developing well constrained depth-age scales for ice cores from temperate glaciers where high melt rates can result in modification of the geochemical record.

The South Cascade Glacier is a low elevation temperate glacier located in the Cascade Mountains of north central Washington State, USA. Ice cores have not previously been retrieved in this region due to high melt rates resulting in meltwater percolation and potentially poor preservation of the paleorecord. In 1994 the United States Geological Survey retrieved a 158 m long ice core from the South Cascade Glacier (2050 m a.s.l.), but the ice core was never processed. We analysed the ice core in 2013, and constrained the depth age scale using a combination of ^{3}H dating [1], ^{210}Pb dating [2, 3], glacial mass balance records [4], annual layer counting and a glacier flow model [5].

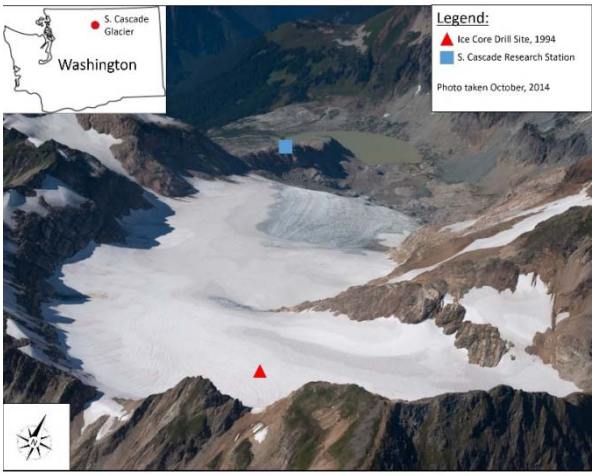

Fig. 1: The South Cascade Glacier, Washington, USA.

^{3}H, associated with atmospheric hydrogen bomb testing, shows a preserved horizon at 27.5 m w.e. core depth, attributed to 1963. Annual glacier mass balance data spanning 1953-1994 from the United States Geological Survey combined with annual layer counting was used to constrain the age of the ice core to 1953±8 at 40 m w.e.. Below this depth annual layer counting was applied using black carbon and stable isotopes, however diffusion of the isotope record due to melt led to high uncertainties below 61 m w.e.. At 61 m w.e. depth the ice core was dated to 1938±14.

We applied ^{210}Pb dating to constrain the age of the deeper portions of the ice core. The ^{210}Pb activity was highly variable with depth, likely due to variable dust deposition. Additionally, the ^{210}Pb record never reached typical ^{210}Pb background levels (3 mBq/kg), likely due to melt water percolation that transported soluble ^{210}Pb downwards, leading to more modern ^{210}Pb being displaced deeper in the glacier. This melt water displacement combined with minimal glacier thinning with depth may account for the observed ^{210}Pb record. Because background ^{210}Pb values were not reached, we are not able to use the ^{210}Pb to constrain the depth-age scale. To fit the ^{210}Pb record to the dating based on ^{3}H, mass balance and annual layer counting required using the -2σ ^{210}Pb age, which indicates the bottom age of the ice core would be 1866 AD with large dating uncertainties. We also present the Nye glacier flow model constrained by the 1963 ^{3}H horizon. The Nye model predicts older dates than the ^{210}Pb dating, however the Nye model will result in an overestimate of the depth-age scale since this model is applicable for cold based glaciers where greater thinning occurs with depth.

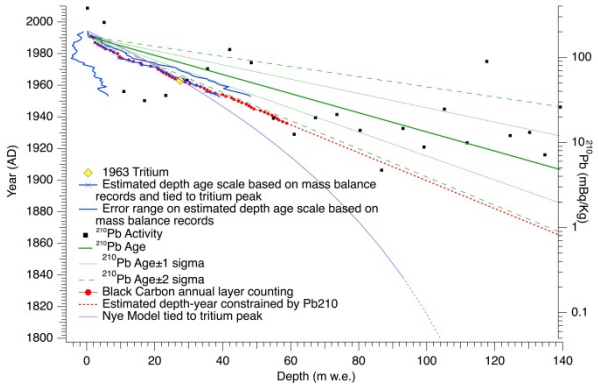

Fig. 2: South Cascade Glacier ice core depth-age scale.

This ice core was analyzed for black carbon and gravimetric impurities to examine the role that light absorbing impurities (LIA) have played in glacier retreat in this region. The uncertainties in the depth-age scale introduce challenges; however the ice core still provides valuable information about variations LIA deposition with time.

This project was supported by the United States Geological Survey and State of Washington Water Research Grant (2013WA372B), the Oeschger Center for Climate Change Research and a Swiss National Science Foundation short visit (IZK0Z2_160953).

[1] U. Morgenstern & C. B. Taylor, Isotopes in Environmental and Health Studies **45**, 96-117 (2009).
[2] A. Eichler, et al., J. Glaciology **46**, 507-515 (2000).
[3] H. W. Gäggeler, et al., J. Glaciology **29,** 165-177 (1983).
[4] L. A. Rasmussen, Ann. Glaciol. **50**, 215-220 (2009).
[5] J. F. Nye, J. Glaciology **4**, 785-788 (1963).

PRESENT HIGH Hg LEVELS ARE DRIVEN BY COAL BURNING IN ASIA

S. Eyrikh (IWEP), A. Eichler, L. Tobler (PSI), N. Malygina, T. Papina (IWEP), M. Schwikowski (PSI & Univ. Bern)

A 300 years record of Hg concentrations from Belukha glacier in the Siberian Altai suggests highest Hg concentrations at the end of the 20th century. This is due to increased Hg emissions from coal burning in Asia outpacing emissions from commercial Hg use.

Mercury (Hg) is a global pollutant causing harm to humans and ecosystems worldwide. Due to the long life time of its elemental form (~1 year), Hg can be transported and distributed globally via the atmosphere or oceans and contaminate environments far away from anthropogenic emission sources. Large uncertainties exist, however, in quantifying and modelling the relevance of Hg emissions from different anthropogenic sources: commercial Hg use and fossil fuel (mainly coal) combustion [1].

Here we present a Hg record from Belukha glacier in the Siberian Altai for the period 1680-2001. Total Hg concentrations in the ice core were analysed by atomic fluorescence spectrometry [2].

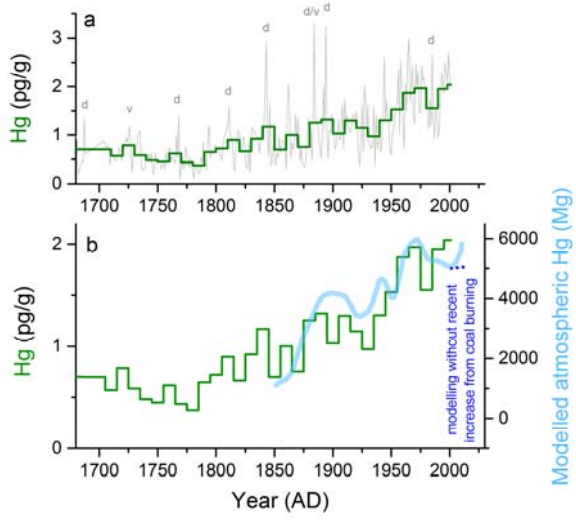

Fig. 1: 10-year mean Belukha Hg record (green) together with **a)** annual averages (grey) (concurrent with high dust concentrations (d) or volcanic layers (v), **b)** modelled atmospheric Hg (light blue, the dark blue line represents modelling without considering recent increases in Hg emissions from coal burning) [1].

Short-term changes in ice-core Hg can be partly related to dust or volcanic input (Fig. 1a). The long-term record shows increasing values until the 1970s, a drop in the 1980s and again high values during 1990-2001. Concentration levels are in the same order of magnitude as in firn and ice from the Tibetan Plateau, Canada, Canadian Arctic, and Greenland and general trends agree (Fig. 2). This indicates that long-term changes of Hg levels in the Altai are mainly determined by global Hg sources. Consequently, Hg concentrations follow closely modelled global atmospheric Hg during the past 150 years (Fig. 1b). Generally, peaks in the 1970s represented at many ice core sites are related to emissions from commercial Hg use (Chlor-alkali industry, batteries, etc.), which declined during the 1980s [1]. High Hg levels at the end of the 20th century can only be explained by rising emissions from coal combustion in Asia. Unlike our record, other ice core records ended too early to capture the recent increase, except the Arctic sites (Fig. 2). Our results imply that emissions from coal burning have to be taken into account when quantifying and modelling present day Hg levels.

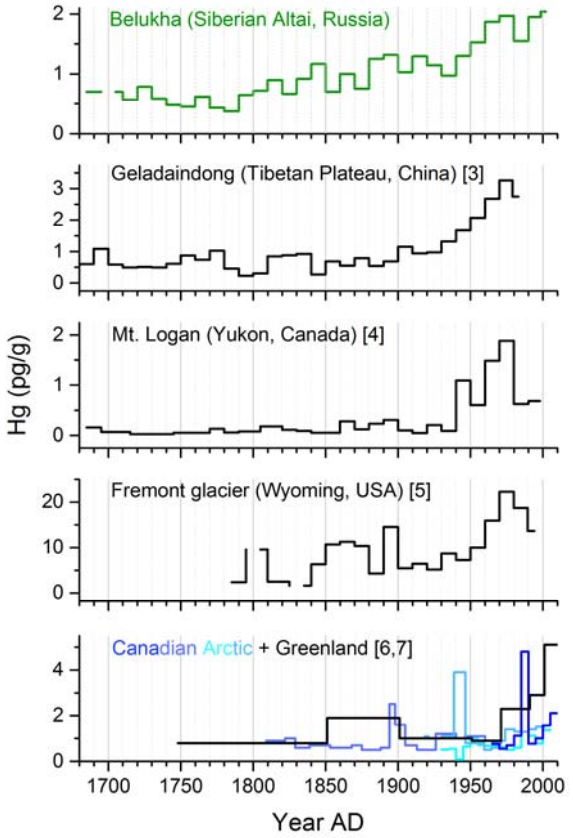

Fig. 2: Worldwide ice-core Hg records.

[1] H.M. Horowitz et al., ES&T, **48**, 10242-10250 (2014).
[2] S. Eyrikh et al., Annual Report Lab. of Radio- & Environm. Chem. PSI & Univ. Bern, 27 (2013).
[3] S. Kang et al., ES&T, **50**, 2859-2869 (2016).
[4] S.A. Beal et al., ES&T, **49**, 7641-7647 (2015).
[5] P.F. Schuster et al., ES&T, **36**, 2303-2310 (2002).
[6] C.M. Zdanowicz et al., Global Biogeochem. Cycles, **30**, 1324-1347 (2016).
[7] J. Zheng, STOTEN., **509-10**, 133-144 (2015).

300 YEARS OF ENSO VARIABILITY RECORDED IN THE MERCEDARIO ICE CORE

T. M. Jenk, A. Ciric, L. Tobler, H. W. Gäggeler (PSI), U. Morgenstern (GNS), G. Casassa (Geoestudios & Univ. Magallanes), M. Lüthi (Univ. Zurich), J. Schmitt (KUP), M. Schwikowski (PSI & Univ. Bern)

Direct linkage between ice core stable isotopes of water, chemical impurity concentrations and the El Niño-Southern Oscillation (ENSO) observed.

South America is a key region for the understanding of climate dynamics in the Southern Hemisphere. With the amount of winter precipitation in Central Chile being significantly correlated to the Southern Oscillation Index, a signal of ENSO can be expected in ice from glaciers located south of the arid belt (28°S to 35°S). This area is strongly influenced by the Westerlies and exhibits a pronounced north to south gradient in precipitation increasing from 300 mm (30°S) to more than 3000 mm (35°S) [1, 2, 3].

In 2005, an ice core was dirlled to a depth of 104 m on La Ollada glacier, Cerro Mercedario, Argentina (31°58‘S, 70°07‘W, 6100 m asl). Borehole temperatures were the lowest measured in the Andes to date and a well preserved ice archive without any melt features was received. The core was dated by a combination of independent methods including annual layer counting, nuclear dating (^{210}Pb, ^{3}H, ^{14}C of WIOC) and trace gas measurements (CH_4, N_2O, CFCs) [4]. The age at 104 m depth was determined with 330 ± 25 year and the mean annual accumulation rate is 0.27 ± 0.03 m w.e., allowing for a seasonal resolution.

Based on typical aerosol lifetimes, daily seven day back trajectory frequencies were modeled for summer and winter of years with either normal, strong La Niña or strong El Niño conditions (NCAR/NCEP data, HYSPLIT model [5]). The major source region of air masses arriving at the drill site is in the Pacific Ocean, east of the central Chilean coast. During austral winter, the marine origin is even more pronounced (slight N-E shift). This shift is strongest for years with strong El Niño conditions and strengthened Westerlies but generally the difference is rather small between seasons as well as between different ENSO conditions. The absence of a significant anthropogenic signal in chemical impurities (e.g. SO_4^{2+}, NH_4^{+}) points to a remote, clean site in agreement with the modeled oceanic source region and the trajectory pathways not crossing any highly populated areas.

A notable covariance between records of chemical impurities and $\delta^{18}O$ exists. Untypically, the undulations in these tracers are not related to seasonality but occur at a multi-annual frequency (Fig. 1a). Principal component analysis results with two main components explaining close to 90% of the total variance. PC1 (81%) with highest loading in sea salt components (Na^+, Cl^-) is significantly correlated with $\delta^{18}O$ (R^2=0.6) suggesting a common marine signal. PC2 (7%) has a higher frequency and highest loading in tracers related to dust (Mg^{2+}, Ca^{2+}).

Wavelet analysis of the seasonal $\delta^{18}O$ record shows significant variance for the typical 20th century ENSO periodicity of 2 – 8 years. Highest correlation with sea surface temperatures (SST, ERSST v3b2, [6]) is observed for waveforms of the 5 – 8 year frequency band (Fig. 1b). Notable shifts in the Merdecdario $\delta^{18}O$ signal periodicity are observed around 1880 and towards longer periods around 1790. The spatial correlation distribution between annual $\delta^{18}O$ and SST indicates the Mercedario $\delta^{18}O$ signal to be related strongest to the NINO3 region (Fig. 1c).

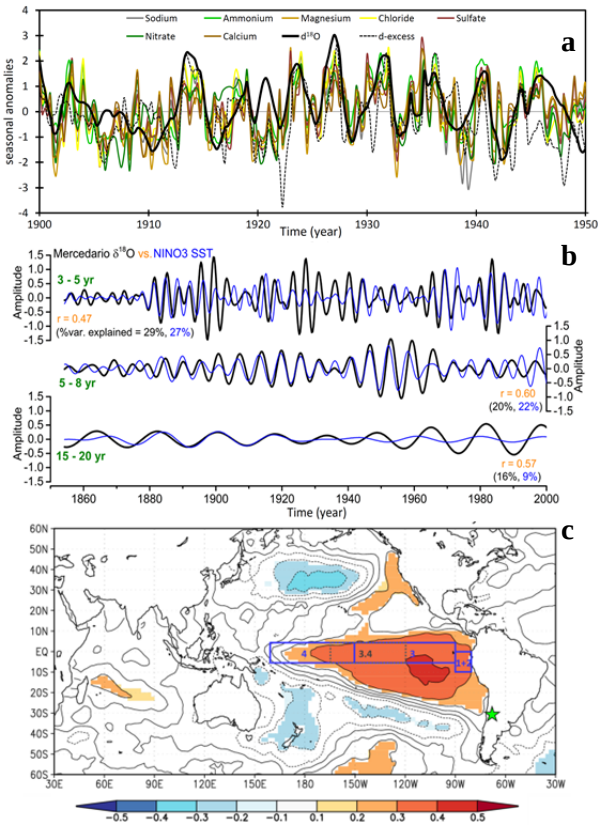

Fig. 1: a) Records of chemical impurities, $\delta^{18}O$ and d-excess for a selected 50 year time period. b) Waveforms of $\delta^{18}O$ and NINO3 SST for selected frequency bands. c) Spatial correlation distribution between annual $\delta^{18}O$ and SST (1870-2004, performed in [6]).

[1] R.D. Garreaud, Adv. Geosci., **22**, 3-11 (2009).
[2] A. Montecinos & P. Aceituno, J. Climate, **16**, 281-296 (2003).
[3] H. Veit, Geographische Rundschau, **52** (2000).
[4] T. M. Jenk et al., Ann. Rep. Lab. of Radio- & Environ. Chem., PSI & Univ. Bern, p. 23 (2014).
[5] R.R. Draxler & G.D. Rolph, NOAA, http://ready.arl.noaa.gov/HYSPLIT.php.
[6] Climate Explorer, www.http://climexp.knmi.nl.

DETERMINATION OF ACCUMULATION RATES IN WEST ANTARCTICA

A. Eichler (PSI), Ch. Pandit (Univ. Bern), S. Brütsch (PSI), A. Rivera, R. Zamora (CECS), M. Schwikowski (PSI & Univ. Bern)

For understanding and modelling recent glacier retreat in West Antarctica, the knowledge of regional climate is crucial. We sampled and dated a 12 m firn core and reconstructed annual accumulation rates.

The West Antarctic Ice Sheet (WAIS) is inherently unstable, losing mass at an increasing rate. It has been hypothesised that a total collapse of the WAIS could raise sea levels by approximately 3.3 m [1]. In particular, the triple ice divide between Pine Island Glacier, Institute Ice Stream and Rutford Ice Stream (PIR divide) is of interest, since a substantial volume of the West Antarctic ice drains via these glaciers [2]. However, little is known about potential causes of glacier retreat and sparse data exist on changes of accumulation rates in this region.

A first reconnaissance study at the PIR divide was performed in January 2014 (79°07'10.4339" S, 88° 50' 21.0634"W, 2083.3 m asl) [3]. The 7 m firn core covered the time period 1997 – 2014 and a mean annual accumulation rate of 25.1 cm weq. was estimated. However, the firn core partly melted during the transport from Antarctica to PSI, disturbing the chemical information originally stored in the core. Thus, the dating and the inferred accumulation rate might be inaccurate.

A new 12 m firn core was drilled at the same site in December 2014 by a team from CECS. The firn core was cut into 324 samples at -20°C in the cold room of the PSI and analyzed for major ions and water stable isotopes. Unusual high concentrations of many species and an abnormal shape occurred on top of each firn core segment (see Fig. 1). We assume that snow debris from the drilling procedure was not sufficiently removed. Hence, from the 12 m firn core we had to remove ~ 90 cm, which did not belong to the actual core, but consisted only of drilling snow debris.

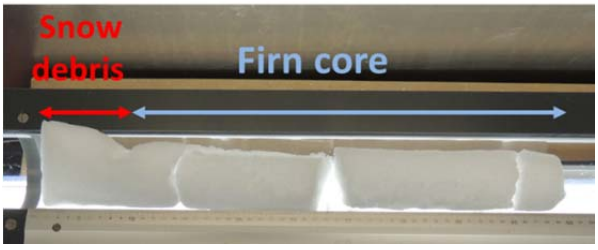

Fig. 1: Image of core 4 of the PIR December 2014 drilling. The remains of the snow debris from drilling on top of the firn core are indicated.

To date the firn core we investigated the seasonality of major ions and water stable isotopes. We distinguished species peaking in summer ($\delta^{18}O$, δD, and marine biogenic derived MSA, SO_4^{2-}, and NO_3^-) and in winter (sea salt species Cl^-, Na^+, K^+, and Mg^{2+}). Dating was performed using these seasonally varying signals and refined with the help of reference horizons (Cl^- peak in winter 2008, volcanic horizons from Pinatubo 1992, Cerro Hudson 1991, and Chaiten 2008) [4] (Fig. 2). Based on this the firn core contains the period 1986 to 2014, with a dating uncertainty of ± 1 year.

We estimated a mean annual accumulation rate of 21.6 ± 4.7 cm weq./year. This is in good agreement with stake measurements and the reconnaissance study.

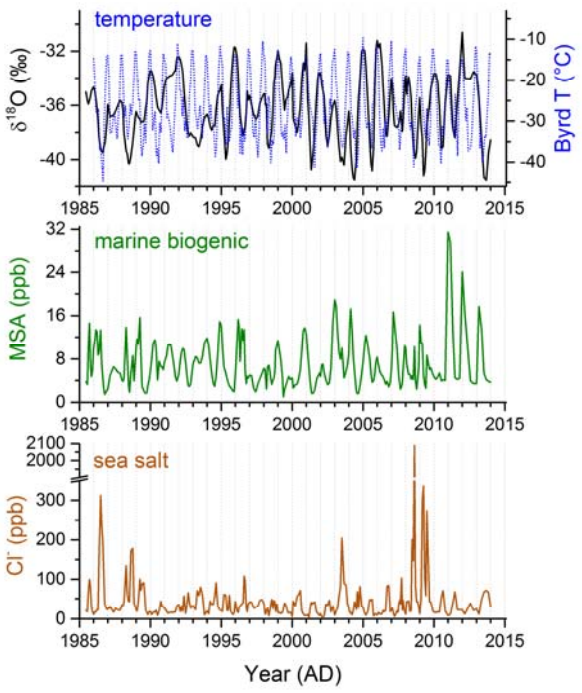

Fig. 2: PIR records of $\delta^{18}O$ (compared to T measurements from the closeby Byrd station), MSA, and Cl^-.

In this work several parameters for the reconstruction of past accumulation from the PIR firn core records have been considered. Future work will include testing the potential of stable isotope and major ion records as climate proxies. To investigate whether $\delta^{18}O$ can be used as a proxy for temperature, we directly compared it with instrumental temperature data from the nearby Byrd station (Fig. 2). However, only 20% of the variability of $\delta^{18}O$ is due to changes in temperature. Furthermore, records of sea salt ions and biogenic species will be evaluated as proxy for wind speed and sea ice extent, respectively.

[1] J. L. Bamber et al., Science, **324**, 901–903 (2009).
[2] P. Dutrieux et al., Science, **343**, 174-178 (2014).
[3] J. Fenwick, Master Thesis, Univ. Bern (2014).
[4] C. Pandit, Master Thesis, Univ. Bern (2016).

^{239}Pu AND ^{236}U FROM EASTERN TIEN SHAN, CHINA

C. Wang (Univ. Nanjing & PSI), H. W. Gäggeler (PSI), S. Hou, H. Pang (Univ. Nanjing), Y. Liu (CAS), M. Christl, H. A. Synal (ETHZ)

Anthropogenic radioactive elements have been released by human activities. ^{239}Pu and ^{236}U deserve special attention due to their high radiological toxicity and long persistence in the environment. Since the first nuclear weapons test in 1945, ^{239}Pu and ^{236}U have been dispersed into the environment. In addition, ^{236}U has been used recently to study marine processes, however its global depositon rate is poorly known.

In 2005, a 57.6 m ice core to bedrock was collected from a dome on the Miaoergou glacier, eastern Tien Shan, Central Asia (43°03'19"N, 94°19'21"E, 4512 m a.s.l.). The low borehole temperature at the drilling site (-7.2 °C at 10 m depth and -8.2 °C at the bottom) is beneficial for the preservation of ice core records [1]. The age-depth relationship of the upper 42.4 m w. e. of the core was established by the combination of annual layer counting, ^{210}Pb dating and detection of the nuclear test time marker (beta activity) [1, 2, 3]. The core segments from 8 to 15 meter depth corresponding to the period between about 1940 and 1970 [2] were selected for the analysis of ^{239}Pu and ^{236}U with the compact low energy system Tandy accelerator mass spectrometer at the Laboratory of Ion Beam Physics, ETH Zürich [4]. The measured concentrations of ^{239}Pu and ^{236}U are shown in Fig. 1. The two peaks represent the maxima in above ground nuclear testing periods in 1958 and 1963, respectively.

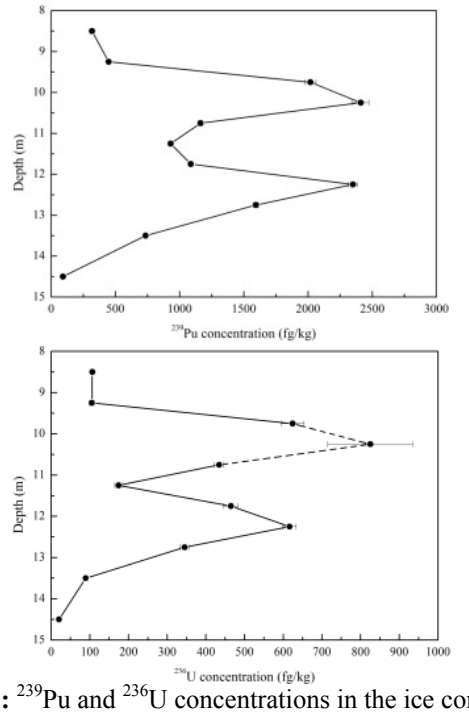

Fig. 1: ^{239}Pu and ^{236}U concentrations in the ice core.

From the concentrations and the diameter of the core the deposition rates were determined. The measured total deposition of ^{239}Pu integrated over the nuclear weapons testing period (NWT) amounts to 1.55 x 10^9 atoms·cm^{-2} (Tab. 1). This value is higher compared to values reported for glaciers from the European Alps with 0.9 x 10^9 atoms·cm^{-2} at Col du Dome, Mt. Blanc, France and 0.7 x 10^9 atoms·cm-2 at Colle Gnifetti, Swiss Alps [5], but lower than 3.6 x 10^9 atoms·cm^{-2} obtained for Belukha glacier, Altai (Russia) [6]. Other literature values are 1.7 x 10^9 measured in a Greenland ice core [7] or 0.54 x 10^9 at the Agassiz ice cap [8], respectively. In a recent publication [9] a comparison was made between ^{239}Pu concentration in Arctic and Antarctic samples, indicating that they differ by about a factor of three (Northern Hemisphere to Southern Hemisphere ratio). The maximum value for ^{239}Pu from several Arctic sites (about 5 mBq kg^{-1}) agrees well with our maximum value of 5.5 mBq kg^{-1} (which corresponds to 2400 fg/kg^{-1}, see Fig. 1). A total fallout of ^{236}U from NWT with the value of 3.5x10^8 atoms·cm^{-2} is consistent with 1.63 x 10^8 atoms·cm^{-2} [10] from the Arctic site Svalbard 79.83°N considering the expected trend of deposition rate with latitude.

Tab. 1: Total flux of ^{239}Pu during NWT from different ice core records.

Site	*Latitude*	*Longitude*	*Total Flux (atoms·cm^{-2})*
Miaoergou	*43°03'19''N*	*94°19'21''E*	*1.55 x 10^9*
Col du Dome	*45°50'N*	*6°50'E*	*0.9 x 10^9*
Colle Gnifetti	*45°55'50.4''N*	*07°52'33.5''E*	*0.7 x 10^9*
Belukha	*49°48'26''N*	*86°34'43''E*	*3.6 x 10^9*
Agassiz	*80°42'N*	*73°06'W*	*0.54 x 10^9*
Greenland	*65°11'N*	*43°50'W*	*1.7 x 10^9*

[1] Y. Liu et al., J. Geophys. Res., **116**, D12307 (2011).
[2] C. Wang et al., Ann. Glaciol. **55,** 105-110 (2014).
[3] C. Wang et al., Ann. Glaciol. **57, 71**, 265-272 (2016).
[4] M. Christl et al., Nucl. Instr. Meth. B, **294**, 29-38 (2013).
[5] J. Gabrieli et al., AE., **45**, 587-593 (2011).
[6] S. Olivier et al., ES&T., 38(24), 6507-6512 (2004).
[7] M. Koide et al., Earth Planet. Sci. Lett., **72**, 1-8 (1982).
[8] A. Kudo et al., Water Sci. Technol., **42**, 163-169 (2000).
[9] M. Arienzo et al., ES&T., **50** (13), 7066-7073 (2016).
[10] C. Wendel et al., Sci. Total Environ., **461-462**, 734-741 (2013).

LIST OF PUBLICATIONS

SURFACE CHEMISTRY

T. Berkemeier, M. Ammann, T. F. Mentel, U. Pöschl, M. Shiraiwa
Organic nitrate contribution to new particle formation and growth in secondary organic aerosols from α-pinene ozonolysis
Environ. Sci. Technol. **50** (12): 6334-6342, doi: 10.1021/acs.est.6b00961 (2016).

T. Berkemeier, S. S. Steimer, U. K. Krieger, T. Peter, U. Poschl, M. Ammann, M. Shiraiwa
Ozone uptake on glassy, semi-solid and liquid organic matter and the role of reactive oxygen intermediates in atmospheric aerosol chemistry
Phys. Chem. Chem. Phys., doi: 10.1039/C6CP00634E (2016).

L. González Palacios, P. Corral Arroyo, K. Z. Aregahegn, S. S. Steimer, T. Bartels-Rausch, B. Nozière, C. George, M. Ammann, R. Volkamer
Heterogeneous photochemistry of imidazole-2-carboxaldehyde: HO_2 radical formation and aerosol growth
Atmos. Chem. Phys. **16** (18): 11823-11836, doi: 10.5194/acp-16-11823-2016 (2016).

P. S. J. Lakey, T. Berkemeier, M. Krapf, J. Dommen, S. S. Steimer, L. K. Whalley, T. Ingham, M. T. Baeza-Romero, U. Pöschl, M. Shiraiwa, M. Ammann, D. E. Heard
The effect of viscosity and diffusion on the HO_2 uptake by sucrose and secondary organic aerosol particles
Atmos. Chem. Phys. **16** (20): 13035-13047, doi: 10.5194/acp-16-13035-2016 (2016).

M.-T. Lee, F. Orlando, L. Artiglia, S. Chen, M. Ammann
Chemical composition and properties of the liquid–vapor interface of aqueous C1 to C4 monofunctional acid and alcohol solutions
J. Phys. Chem. A **120** (49): 9749-9758, doi: 10.1021/acs.jpca.6b09261 (2016).

G. Li, H. Su, X. Li, U. Kuhn, H. Meusel, T. Hoffmann, M. Ammann, U. Pöschl, M. Shao, Y. Cheng
Uptake of gaseous formaldehyde by soil surfaces: a combination of adsorption/desorption equilibrium and chemical reactions
Atmos. Chem. Phys. **16** (15): 10299-10311, doi: 10.5194/acp-16-10299-2016 (2016).

F. Orlando, A. Waldner, T. Bartels-Rausch, M. Birrer, S. Kato, M. T. Lee, C. Proff, T. Huthwelker, A. Kleibert, J. A. van Bokhoven, M. Ammann
The environmental photochemistry of oxide surfaces and the nature of frozen salt solutions: A new in situ XPS approach
Top. Catal. **59** (5-7): 591-604, doi: 10.1007/s11244-015-0515-5 (2016).

ANALYTICAL CHEMISTRY

S. Crespo, J. Aranibar, L. Gomez, M. Schwikowski, S. Brütsch, L. Cara, R. Villalba
Ionic and stable isotope chemistry as indicators of water sources to the Upper Mendoza River basin, Central Andes of Argentina
Hydrological Sciences Journal: 1-18, doi: 10.1080/02626667.2016.1252840 (2016).

P. Froidevaux, F. Bochud, S. Baechler, V. Castella, M. Augsburger, C. Bailat, K. Michaud, M. Straub, M. Pecchia, T. M. Jenk, T. Uldin, P. Mangin
^{210}Po poisoning as possible cause of death: Forensic investigations and toxicological analysis of the remains of Yasser Arafat
Forensic Sci. Int. **259**: 1-9, doi: 10.1016/j.forsciint.2015.09.019 (2016).

P. Gabrielli, C. Barbante, G. Bertagna, M. Bertó, D. Binder, A. Carton, L. Carturan, F. Cazorzi, G. Cozzi, G. Dalla Fontana, M. Davis, F. De Blasi, R. Dinale, G. Dragà, G. Dreossi, D. Festi, M. Frezzotti, J. Gabrieli, S. P. Galos, P. Ginot, P. Heidenwolf, T. M. Jenk, N. Kehrwald, D. Kenny, O. Magand, V. Mair, V. Mikhalenko, P. N. Lin, K. Oeggl, G. Piffer, M. Rinaldi, U. Schotterer, M. Schwikowski, R. Seppi, A. Spolaor, B. Stenni, D. Tonidandel, C. Uglietti, V. Zagorodnov, T. Zanoner, P. Zennaro
Age of the Mt. Ortles ice cores, the Tyrolean Iceman and glaciation of the highest summit of South Tyrol since the northern hemisphere climatic optimum
The Cryosphere **10** (6): 2779-2797, doi: 10.5194/tc-10-2779-2016 (2016).

F. Inceoglu, M. F. Knudsen, J. Olsen, C. Karoff, P. A. Herren, M. Schwikowski, A. Aldahan, G. Possnert
A continuous ice-core Be-10 record from Mongolian mid-latitudes: Influences of solar variability and local climate
Earth. Planet. Sci. Lett. **437**: 47-56, doi: 10.1016/j.epsl.2016.01.006 (2016).

T. M. Jenk, M. Rubino, D. Etheridge, V. G. Ciobanu, T. Blunier
A new set-up for simultaneous high-precision measurements of CO_2, $\delta^{13}C$-CO_2 and $\delta^{18}O$-CO_2 on small ice core samples
Atmos. Meas. Tech. **9** (8): 3687-3706, doi: 10.5194/amt-9-3687-2016 (2016).

E. S. Klein, M. Nolan, J. McConnell, M. Sigl, J. Cherry, J. Young, J. M. Welker
McCall Glacier record of Arctic climate change: Interpreting a northern Alaska ice core with regional water isotopes
Quat. Sci. Rev. **131, Part B**: 274-284, doi: 10.1016/j.quascirev.2015.07.030 (2016).

C. Müller-Tautges, A. Eichler, M. Schwikowski, G. B. Pezzatti, M. Conedera, T. Hoffmann
Historic records of organic compounds from a high Alpine glacier: Influences of biomass burning, anthropogenic emissions, and dust transport
Atmos. Chem. Phys. **16** (2): 1029-1043, doi: 10.5194/acp-16-1029-2016 (2016).

M. Sigl, T. J. Fudge, M. Winstrup, J. Cole-Dai, D. Ferris, J. R. McConnell, K. C. Taylor, K. C. Welten, T. E. Woodruff, F. Adolphi, M. Bisiaux, E. J. Brook, C. Buizert, M. W. Caffee, N. W. Dunbar, R. Edwards, L. Geng, N. Iverson, B. Koffman, L. Layman, O. J. Maselli, K. McGwire, R. Muscheler, K. Nishiizumi, D. R. Pasteris, R. H. Rhodes, T. A. Sowers
The WAIS Divide deep ice core WD2014 chronology – Part 2: Annual-layer counting (0–31 ka BP)
Clim. Past **12** (3): 769-786, doi: 10.5194/cp-12-769-2016 (2016).

C. Steinlin, C. Bogdal, M. P. Lüthi, P. A. Pavlova, M. Schwikowski, M. Zennegg, P. Schmid, M. Scheringer, K. Hungerbühler
A temperate alpine glacier as a reservoir of polychlorinated biphenyls: Model results of incorporation, transport, and release
Environ. Sci. Technol. **50** (11): 5572-5579, doi: 10.1021/acs.est.5b05886 (2016).

C. Uglietti, A. Zapf, T. M. Jenk, M. Sigl, S. Szidat, G. Salazar, M. Schwikowski
Radiocarbon dating of glacier ice: overview, optimisation, validation and potential
The Cryosphere **10** (6): 3091-3105, doi: 10.5194/tc-10-3091-2016 (2016).

C. P. Vega, V. A. Pohjola, E. Beaudon, B. Claremar, W. J. J. van Pelt, R. Pettersson, E. Isaksson, T. Martma, M. Schwikowski, C. E. Bøggild
A synthetic ice core approach to estimate ion relocation in an ice field site experiencing periodical melt: A case study on Lomonosovfonna, Svalbard
The Cryosphere **10** (3): 961-976, doi: 10.5194/tc-10-961-2016 (2016).

C. P. Vega, E. Schlosser, D. V. Divine, J. Kohler, T. Martma, A. Eichler, M. Schwikowski, E. Isaksson
Surface mass balance and water stable isotopes derived from firn cores on three ice rises, Fimbul Ice Shelf, Antarctica
The Cryosphere **10** (6): 2763-2777, doi: 10.5194/tc-10-2763-2016 (2016).

Y. Zhang, S. Kang, B. Grigholm, Y. Zhang, S. Kaspari, U. Morgenstern, J. Ren, D. Qin, P. A. Mayewski, Q. Zhang, Z. Cong, M. Sillanpää, M. Schwikowki, F. Chen
Twentieth-century warming preserved in a Geladaindong mountain ice core, central Tibetan Plateau
Ann. Glaciol. **57** (71): 70 - 80, doi: 10.3189/2016AoG71A001 (2016).

AFFILIATION INDEX

CECS	Centro de Estudios Científicos, Aturo Prat 514, Valdivia, Chile
CAS	Chinese Academy of Sciences, 52 Sanlihe Rd., Beijing 100864 , China
CWU	Central Washington University, 400 E. University Way Ellensburg, WA 98926, USA
Czech AS	The Czech Academy of Sciences, Národní 3, 117 20 Praha 1, Czech Republic
ETHZ	Eidgenössische Technische Hochschule Zürich, 8092 Zürich, Switzerland
Geoestudios	Los Aromos 3408, Las Vertientes, San Jose de Maipo Santiago, Chile
GNS	Institute of Geological and Nuclear Sciences, National Isotope Centre, Lower Hutt 5040, New Zealand
IRCELYON	Institut de recherches sur la catalyse et l'environnement de Lyon, 2 avenue Albert Einstein, 69626 Villeurbanne cedex, France
IWEP	Institute for Water and Environmental Problems, 1, Molodyoznaya St., Barnaul 656038, Altai Krai, Russia
KUP	Climate and Environmental Physics, Physics Institute, University of Bern, Sidlerstrasse 5, 3012 Bern, Switzerland
LBL	Lawrence Berkeley National Laboratory, One Cyclotron Road, Berkeley, CA 94720, USA
MPIC	Max-Planck-Institut für Chemie (Otto-Hahn-Institut), Joh.-Joachim-Becher-Weg 27, 55128 Mainz, Germany
NPI	Norwegian Polar Institute, 9296 Tromsø, Norway
NTNU	Norwegian University of Science and Technology, 7491 Trondheim, Norway
PSI	Paul Scherrer Institut, 5232 Villigen, Switzerland
SNF	Schweizerischer Nationalfonds SNF, Wildhainweg 3, 3001 Bern, Switzerland
UCI	University of California, Irvine, Department of Earth System Science, Croul Hall, Irvine, CA 92697-3100, USA
UiB	University of Bergen, 5020 Bergen, Norway
Univ. Bern	Departement für Chemie und Biochemie, Universität Bern, Freiestrasse 3, 3012 Bern, Switzerland
Univ. Bern/IPS	Institute of Plant Sciences, Altenbergrain 21, 3013 Bern, Switzerland
Univ. Gothenburg	University of Gothenburg, Vasaparken, 405 30 Gothenburg, Sweden
Univ. Lille 1	Université de Lille 1 Sciences et Technologies, Cité Scientifique, 59655 Villeneuve d'Ascq Cédex, France
Univ. Lyon	Université de Lyon, 92 rue Pasteur, 69361 Lyon cedex 07, France
Univ. Magallanes	University of Magallanes, Punta Arenas 6210427, Chile
Univ. Nanjing	School of Geographic and Oceanographic Sciences, Nanjing University, 163 Xianlin Road, Nanjing 210023, China
Univ. Zurich	University of Zurich, Department of Geography, 8057 Zurich, Switzerland
USC	University of Southern California, Los Angeles, CA 90089, USA
WSL-SLF	WSL-Institute for Snow and Avalanche Research SLF, Flüelastrasse 11, 7260 Davos Dorf, Switzerland
XMU	Xiamen University, 422, Siming South Road, Xiamen, Fujian, 361005, China

Paul Scherrer Institut :: 5232 Villigen PSI :: Switzerland :: Tel. +41 56 310 21 11 :: Fax +41 56 310 21 99 :: www.psi.ch